國 立 交 通 大 學

電信工程學系碩士班
碩士論文

使用鏈路調節與多輸入多輸出編碼改善
正交分頻多工無線網路效能之研究

Throughput Enhancement via Link Adaptation and
MIMO Coding in OFDM-Based WLANs

研 究 生：曹祐瑞　　Student: Yu-Jui Tsao

指導教授：李大嵩 博士　　Advisor: Dr. Ta-Sung Lee

中 華 民 國 九 十 三 年 六 月

使用鏈路調節與多輸入多輸出編碼改善正交分頻多工無線網路效能之研究

Throughput Enhancement via Link Adaptation and MIMO Coding in OFDM-Based WLANs

研 究 生：曹祐瑞　　Student: Yu-Jui Tsao

指導教授：李大嵩 博士　　Advisor: Dr. Ta-Sung Lee

國立交通大學

電信工程學系碩士班

碩士論文

A Thesis
Submitted to Institute of Communication Engineering
College of Electrical Engineering and Computer Science
National Chiao Tung University
in Partial Fulfillment of the Requirements
for the Degree of
Master of Science
in
Communication Engineering
June 2004
Hsinchu, Taiwan, Republic of China

中 華 民 國 九 十 三 年 六 月

使用鏈路調節與多輸入多輸出編碼改善正交分頻多工無線網路效能之研究

學生：曹祐瑞　　指導教授：李大嵩 博士

國立交通大學電信工程學系碩士班

摘要

日益增多的各式無線服務需求，如語音、資料傳輸及多媒體，促進了高速無線區域網路的蓬勃發展。IEEE 802.11 是眾多致力於標準化無線區域網路之媒介存取與實體層的主要力量之一。其中於媒介存取控制層規範了兩種通道存取機制─基本存取機制與請求發送/允許發送存取機制。此外，延伸的 IEEE 802.11a 透過實體層的正交分頻多工技術可實現 6 Mbps 至 54 Mbps 之高速傳輸。在多傳輸速率的系統中，鏈路調節顯得愈加重要，其作用在於可動態地轉換傳輸速率以配合變動之通道狀態。在本論文中，吾人所提出之鏈路調節演算法可更適當地利用 IEEE 802.11a 無線區域網路之媒介存取與實體層。此鏈路調節演算法可根據通道狀態、競爭站台之多寡與資料長度選擇存取機制與傳輸速率之最佳組合以提升固有之無線區域網路效能。再者，多輸入多輸出編碼與正交分頻多工技術之結合被視為提昇新世代無線通訊系統傳輸速率之前瞻技術。依據機能之不同，多輸入多輸出編碼可分為兩類。其中空間分集之作用在於改善鏈路之可靠度，另一方面，空間分工則著墨於增加使用頻譜的效率。吾人對所提出之鏈路調節演算法進行修改，使其可選取適當的多輸入多輸出編碼，以適應當下環境提供良好的鏈路品質或提昇傳輸速率，進而改善無線網路之效能。最後，藉由電腦模擬結果驗證上述方法之表現，吾人可證實其在室內無線環境有優異的效能。

Throughput Enhancement via Link Adaptation and MIMO Coding in OFDM-Based WLANs

Student: Yu-Jui Tsao Advisor: Dr. Ta-Sung Lee

Institute of Communication Engineering

National Chiao Tung University

Abstract

The increasing demand for all types of wireless services (e.g. voice, data, and multimedia) promotes fast growing of the high-speed wireless local area networks (WLANs). One of the major efforts in standardizing the medium access control (MAC) and physical (PHY) layers for WLANs is IEEE 802.11. It defines two channel access mechanisms, the basic and RTS/CTS access mechanism, at the MAC layer. Besides, the extended IEEE 802.11a achieves high data rates ranging from 6 Mbps to 54 Mbps by using orthogonal frequency division multiplexing (OFDM) at the PHY layer. With multiple rates, link adaptation (LA), a process to dynamically switch data rates to best match the varying channel condition, becomes increasingly important. In this thesis, we propose an LA algorithm to better exploit the MAC and PHY layer in the IEEE 802.11a WLAN. According to the channel condition, number of contending stations, and data length, the proposed LA algorithm chooses the optimum combination of the access method and data rate to achieve higher throughput in the inherent IEEE 802.11a WLAN. Furthermore, the combining of multiple-input multiple-output (MIMO) coding with OFDM is regarded as a promising technique for enhancing the data rates of next generation wireless communication systems. The MIMO coding can be categorized into two types based on their functionality. Spatial diversity (SD) is used to improve the link reliability while spatial multiplexing (SM) increases the spectral efficiency. For further improvements in the WLAN's throughput, we modify the proposed LA algorithm so that it can choose the appropriate MIMO coding as well to provide the better link quality or higher data rate according to channel condition. Finally, we evaluate the performance of the proposed algorithms by computer simulations, and confirm that they work well in indoor wireless environments.

Acknowledgement

I would like to express my deepest gratitude to my advisor, Dr. Ta-Sung Lee, for his enthusiastic guidance and great patience. Heartfelt thanks are also offered to all members in the Communication Signal Processing (CSP) Lab for their constant encouragement. Last but not least, I would like to show my sincere appreciation and love to my family for their life-long love and support.

Contents

List of Figures

List of Tables

Abbreviation

ACK	acknowledgement
AWGN	additive white Gaussian noise
BER	bit error rate
BLAST	Bell laboratories layered space-time
BPSK	binary phase shift keying
BSS	basic service set
CSMA/CA	carrier sense multiple access with collision avoidance
CTS	clear-to-send
CW	contention window
DCF	distributed coordination function
DIFS	DCF inter frame space
EIFS	extended inter frame space
FCS	frame check sequence
FEC	forward error correction
FFT	fast Fourier transform
IFS	inter frame space
ISI	inter-symbol interference
LA	link adaptation
MAC	medium access control
MIMO	multiple-input multiple-output

MPDU	MAC protocol data unit
MSDU	MAC service data unit
NAV	network allocation vector
OFDM	orthogonal frequency division multiplexing
PAM	pulse amplitude modulation
PCF	point coordination function
PHY	physical layer
PIFS	PCF inter frame space
PLCP	PHY convergence procedure
PMD	physical medium dependent
PPDU	PLCP protocol data unit
PSDU	PHY service data unit
QAM	quadrature amplitude modulation
QPSK	quadrature phase shift keying
RSH	reservation subheader
RTS:	request-to-send
SIFS	short inter frame space
SISO	single-input single-output
SLRC	station long retry count
SNR	signal-to-noise ratio
SSRC	station short retry count
STBC	space-time block code
U-NII	unlicensed national information infrastructure
VBLAST	vertical BLAST
WLAN	wireless local area network

Notations

$CWmin$	minimum contention window size
$CWmax$	maximum contention window size
$\mathbf{H}_k$	kth-subband MIMO channel matrix
l	data payload length
m	PHY mode
n	number of contending stations
n_l	long retry limit
n_s	short retry limit
n_R	number of receive antennas
n_T	number of transmit antennas
N_0	power spectral density of AWGN
T_{FFT}	FFT interval
T_{GI}	OFDM guard interval
$T_{PREAMBLE}$	duration of the PLCP preamble
T_{SIGNAL}	duration of the SIGNAL field

T_{SYM}	OFDM symbol duration
x	transmitted signal
y	received signal
γ	average received SNR per symbol
$\lambda_{k,\min}$	minimum singular value of $\mathbf{H}_k$
$\left\|\mathbf{H}_k\right\|_F^2$	squared Frobenius norm of $\mathbf{H}_k$

Chapter 1

Introduction

The increasing demand for all types of wireless services (e.g. voice, data, and multimedia) promotes fast growing of high-speed wireless local area networks (WLANs). One of the major efforts in standardizing the medium access control (MAC) and physical (PHY) layers for WLANs is IEEE 802.11 [1].

In IEEE 802.11 MAC, the distributed coordination function (DCF) is the fundamental access method. There are two techniques used for packet transmitting in DCF. The default one is a two-way handshaking mechanism, also known as basic access method. The other optional one is a four-way handshaking mechanism, which uses the request-to-send/clear-to-send (RTS/CTS) technique to reserve the channel before data transmission, also known as RTS/CTS access method. One of the benefits of the RTS/CTS access method is to increase the system performance by minimizing the amount of time wasted when collisions occur on long data frames. However, the RTS/CTS technique also increases two additional overheads without any payload, thus decreasing efficiency. For that reason, the use of the RTS/CTS access method is under the control of the manageable object, RTS_Threshold, which indicates the data length under which the data frames should be sent without RTS/CTS [2][3].

IEEE 802.11a [4] is a high-speed physical layer defined for the 5 GHz U-NII bands as a supplement to the existing IEEE 802.11 WLAN standard. It provides eight

PHY modes with transmission rates ranging from 6 Mbps up to 54 Mbps by using orthogonal frequency division multiplexing (OFDM) [5] as its underlying radio technology.

The mechanism to select one out of multiple available transmission rates at a given time is referred to as link adaptation (LA) [6]. The principle of LA is to adapt the transmission rates to best match the channel conditions in order to achieve one or several performance criteria, like system throughput maximization, bit error rate (BER) ,and etc. LA algorithms for IEEE 802.11 WLANs have been studied by many researchers [7-11]. However, these existing approaches focus on the PHY modes only. The transmission duration of a fixed-length data fluctuates according to the transmission rate. Therefore, RTS_Threshold, the only parameter for deciding whether the RTS/CTS access method is applied, is not sufficient now.

To address this issue, we propose an integrated LA algorithm that better exploits the inherent MAC and PHY layers by choosing the best combination of the MAC access method and PHY mode according to the data frame length, wireless channel condition, and number of contending stations for maximizing the system goodput. Here, the goodput refers to the useful data rate the user actually enjoys after all the overheads are accounted for, including the MAC/PHY overheads, backoff delay, interframe intervals, and the potential frame retransmission times.

Another aim of this thesis is to enhance the performance of the current 802.11a standard by employing multiple antennas at the transmitter and receiver. The combining of multiple-input multiple-output (MIMO) coding with OFDM is considered as a promising technique for enhancing the data rates of next-generation wireless communication systems, especially WLAN systems. An advantage of WLAN systems is that they are mainly deployed in indoor environments. These environments are typically characterized by richly scattered multipaths. As explained in [12], this is a

good condition for having a high MIMO capacity.

MIMO coding techniques can basically be split into two groups: spatial diversity [13], e.g. space-time block code (STBC) [14][15] and spatial multiplexing [12][16][17], e.g. Bell laboratories layered space-time (BLAST) [18][19]. While STBC improves the link quality of the system by exploiting the spatial and temporal diversity, BLAST significantly improves the spectral efficiency of the system at the cost of poor error performance. We compare these two techniques using the performance metric of goodput defined above, and are able to select the most suitable MIMO technique under the given channel condition to increase the link throughput in an MIMO-enhanced 802.11a WLAN system.

The rest of this thesis is organized as follows. In Chapter 2, we introduce the principles of mandatory DCF mechanism of IEEE 802.11 MAC and OFDM characteristics of 802.11a PHY. Based on these understandings, we analyze the goodput performance of the 802.11a systems and propose an integrated LA algorithm for adapting MAC access and PHY mode in Chapter 3. In Chapter 4, we modify the proposed LA algorithm for MIMO-enhanced 802.11a systems. In Chapter 5, we conclude this thesis and propose some potential future works.

Chapter 2

Overview of IEEE 802.11a Systems

In this chapter, we will describe the principles of the IEEE 802.11 MAC in Section 2.1. In Section 2.2, we will introduce some characteristic in IEEE 802.11a PHY, which is an OFDM-based WLAN standard.

2.1 IEEE 802.11 MAC

IEEE 802.11 MAC provides a fair access to the shared wireless medium through two different mechanisms: a mandatory contention-based access protocol, called the distributed coordination function (DCF), and an optional polling-based protocol, called the point coordination function (PCF) [1]. PCF is very rarely implemented in currently available devices. In this thesis, we consider only the DCF protocol, which is prevailing in the market today.

DCF is based on carrier sense multiple access with collision avoidance (CSMA/CA). With CSMA, a station wishing to transmit first listens to the medium to determine if another transmission is in progress (carrier sense). If the medium is in use, the station must wait. If the medium is idle, the station transmits. It may happen that two or more stations attempt to transmit at about the same time. If this happens, there

will be a collision; the data from both transmissions will be disarranged and not received successfully. To reduce the collision probability between multiple stations accessing the wireless medium, collision avoidance (CA) is carried out in two ways: i) by following a backoff procedure before the data transmission, and ii) by keeping track of the expected duration of ongoing transmissions. The latter technique is termed virtual carrier sensing and practically realized by recording the transmission duration information contained in the request-to-send (RTS), clear-to-send (CTS), and data frames.

Under DCF, data frames are transmitted via two methods. The essential method used in DCF is called the basic access method. The 802.11 standard also provides an alternative way of transmitting data frames, namely the RTS/CTS access method

2.1.1 Basic Access Method

In IEEE 802.11, priorities for accessing to the wireless medium are controlled by the use of inter frame space (IFS) intervals, i.e. time intervals between the transmissions of consecutive frames. The standard defines four different IFS intervals: short IFS (SIFS), PCF IFS (PIFS), DCF IFS (DIFS), and extended IFS (EIFS). The SIFS is the smallest followed by PIFS, DIFS, and EIFS. After an SIFS, only acknowledgement (ACK), CTS and data frames may be sent. The use of PIFS and DIFS is to separate the PCF and DCF modes.

Under the basic access method, a station, when starting a new frame transmission, shall sense the wireless medium to determine if another station is transmitting. If the station detects that the wireless medium has been idle for more than a time interval called DIFS, the station can transmit the data frame immediately. If the medium is sensed as busy, the station waits until the channel becomes idle, then defers for an

extra DIFS interval. If the medium remains idle, the MAC starts the backoff procedure by selecting a random backoff count since collisions are most likely to happen just after the medium becomes free. The backoff counter (how to select the random backoff count is detailed below) is decremented as long as the channel is sensed idle, frozen when a transmission is detected on the channel, and reactivated when the channel is sensed idle again for more than a DIFS. The station transmits when the counter reaches zeros.

To select the random backoff count, each station maintains a contention window (CW) value. The backoff count, in the unit of Slot_Time, is determined as a random integer drawn from a uniform distribution over the interval [0, CW]. The value of CW is initially assigned a $CWmin$, and increases exponentially when a transmission fails. After any unsuccessful transmission attempt, another backoff is performed with a new CW value determined as follows:

$$CW \Leftarrow 2 \cdot (CW + 1) - 1 \tag{2.1}$$

The set of CW values are sequentially ascending integer powers of 2 minus 1. Once the CW value reaches the value of $CWmax$, it remains at the value of $CWmax$ until it is reset. The CW value is reset to $CWmin$ after a successful transmission or after reaching the maximum retry limit. If the maximum retry limit ($ShortRetryLimit$ or $LongRetryLimit$) is reached, the retransmission attempts shall cease, and the frame shall be discarded.

Every station maintains a station short retry count (SSRC) as well as a station long retry count (SLRC), both of which have an initial value of zero. SSRC indicates the retransmission number of the RTS frames or the data frames transmitted by the basic access method. SLRC indicates the retransmission number of data frames when

the RTS/CTS technique is used. The specified limits of SSRC and SLRC are $ShortRetryLimit$ and $LongRetryLimit$ (typically 7 and 4), respectively. The SSRC is reset to 0 whenever a CTS is received in response to an RTS or whenever an ACK is received in response to a data frame. The SLRC is also reset to 0 whenever an ACK is received in response to a data frame when the RTS/CTS technique is used.

One important characteristic of the IEEE 802.11 MAC is that an ACK frame shall be transmitted by the receiver after a successful data frame reception. Only after receiving the ACK frame correctly, the transmitter assumes that the data frame was delivered successfully. SIFS, which is smaller than DIFS, is the time interval between the data frame reception and ACK frame transmission. Using this smallest IFS interval between transmissions within the frame exchange sequence prevents other stations, which are required to wait for the medium to be idle for a longer time interval, e.g. at least a DIFS time, from attempting to use the medium, thus giving priority to completion of the frame exchange sequence in progress. If the ACK frame is not received within an ACK_Timeout period after the data transmission, the data frame is retransmitted after another random backoff. When the data frame is correctly transmitted and the corresponding ACK is received, the station performs a DIFS deference and another random backoff process, which is often referred to as "post-backoff" to avoid channel capture.

When a data frame is transmitted, all the other stations hearing the data frame adjust their network allocation vector (NAV), which is used for virtual carrier sensing at the MAC layer indicating the period of time in which the channel will remain busy, based on the duration field value in the data frame, which includes an SIFS interval and the transmission time of the ACK frame following the data frame.

Based on the above discussion, we notice that a transmission cycle under the

basic access method consists of the following phases: the DIFS deferral phase, backoff phase if necessary, data transmission phase, SIFS deferral phase, and ACK transmission phase. The timing of successful frame transmission is illustrated in Figure 2.1(a). In Figure 2.1(b), if no ACK frame is received after an SIFS interval, due possibly to collision or an erroneous reception, i.e. received with an incorrect frame check sequence (FCS), the transmitter will contend again for the medium to retransmit the data frame after an ACK_Timeout. However, if an ACK frame is received in error, the transmitter will recontend for the medium to retransmit the data frame after an EIFS interval, as shown in Figure 2.1(c).

2.1.2 RTS/CTS Access Method

DCF also defines an optional way, named the RTS/CTS access method, of transmitting data frames, which involves the transmission of special short RTS and CTS frames prior to the transmission of the actual data frame. Before transmitting a data frame, the source station reserves the channel by sending an RTS after a DIFS (along with backoff count if necessary) long idle channel. When the receiving station detects an RTS frame, it responds, after an SIFS interval, with a CTS frame. The source station is allowed to transmit its data frame only if the CTS frame is correctly received. If the CTS frame is not received by the source station, it is assumed that a collision occurred and an RTS retransmission is scheduled. After the data frame is received by the receiving station, an ACK frame is sent back to the source, verifying successful data reception.

The RTS and CTS frames carry the information of the duration of frame transmission. This information can be read by any listening station, which is then able to update the NAV containing the information of the time period in which the channel

will remain busy. Therefore, when a station is hidden from either the transmitting or receiving station, by detecting just one frame among the RTS and CTS frames, it can suitably delay further transmission, and thus avoid collision. That is, the successful exchange of small messages, RTS and CTS, reserves the area within the range of the transmitter and receiver for the intended transmission period guaranteeing undisturbed transmission for the longer data frame.

The RTS/CTS access method allows increasing the system performance by minimizing the amount of time wasted when collisions occur on long data frames. More specifically, if a collision occurs with two or more small RTS frames, the time loss is smaller compared to the collision of long data frames. On the other hand, the RTS/CTS technique decreases efficiency since it transmits two additional frames without any payload. For that reason, the use of the RTS/CTS access method is under the control of the manageable object, RTS_Threshold, which indicates the data length under which the data frames should be sent without RTS/CTS. The data frame size is the only parameter that is used to decide whether the mechanism is applied. The RTS_Threshold parameter is not fixed in the IEEE 802.11 standard and has to be set separately by each station.

To summarize the discussion above, a transmission cycle under the RTS/CTS access method consists of the following phases: the DIFS deferral phase, backoff phase if necessary, RTS transmission phase, SIFS deferral phase, CTS transmission phase, SIFS deferral phase, data transmission phase, SIFS deferral phase, and ACK transmission phase. The timing of successful frame transmission is illustrated in Figure 2.2(a). On the other hand, if no CTS frame is received, due possibly to collision or an erroneous reception of the RTS frame, as shown in Figure 2.2(b), or if no ACK frame is received, due possibly to an erroneous reception of the data frame, as shown in Figure 2.2(c), after an SIFS interval, the transmitter will contend again for the medium

to retransmit the RTS frame after a CTS_Timeout or an ACK_Timeout. However, if a CTS or an ACK frame is received in error, the transmitter will recontend for the medium to retransmit the RTS frame after an EIFS interval, as shown in Figure 2.2(d) and Figure 2.2(e), respectively.

2.2 IEEE 802.11a OFDM PHY

The PHY layer is the interface between the MAC layer and wireless medium, which transmits and receives data frames over the shared wireless medium. In order to allow IEEE 802.11 MAC to operate with minimum dependence on the physical medium dependent (PMD) sublayer, a PHY convergence procedure (PLCP) sublayer is defined. The frame exchange between MAC and PHY is under the control of the PLCP sublayer. Figure 2.3 illustrates their relation. During the transmission, the MAC protocol data units (MPDUs) from the MAC layer shall be preceded by a PLCP preamble and a PLCP header to create PLCP protocol data units (PPDUs). The format of the PPDU is shown in Figure 2.4.

IEEE 802.11a is an OFDM-based WLAN standard developed by IEEE 802.11. In July 1998, the IEEE 802.11 standardization group decided to select OFDM as the basis for a new PHY standard extension to the existing 802.11 MAC standard [4]. In the IEEE 802.11a standard, the WLAN system is initially designed to operate in the 5.15-5.35 and 5.725-5.825 GHz unlicensed national information infrastructure (U-NII) bands. There are totally eight non-overlapping 20 MHz channels across the 5.15-5.35 GHz band. The resulting subcarrier frequency spacing is 312.5 kHz (for a 20 MHz with 64 possible subcarrier frequency slots). IEEE 802.11a specifies data rates ranging from 6 to 54 Mbps by using the OFDM technique to achieve high-speed WLAN

communications. Table 2.1 contains a listing of the eight specified PHY modes. Four different modulation schemes are used: binary and quadrature phase shift keying (BPSK/QPSK), 16-quadrature amplitude modulation (16-QAM) and 64-QAM. Each higher performing modulation scheme requires a better channel condition for accurate transmission, making the idea of link adaptation (LA) feasible and important (we will discuss this issue in the later chapter). These modulation schemes are coupled with the various rate forward error correction (FEC) codes. In the IEEE 802.11a standard, the convolutional code is used. The support of transmitting and receiving at the data rates of 6, 12, and 24 Mbps is mandatory in the IEEE 802.11a PHY. The timing parameters associated with the OFDM physical layer is listed in Table 2.2.

2.2.1 OFDM Overview

OFDM [5] is a modulation scheme that converts a wideband signal into a series of independent narrowband signal placed side-by-side in the frequency domain. The main benefit of OFDM is that the subcarriers in the frequency band can actually overlap one-another in the frequency domain for the orthogonal property of subcarriers. The basic idea is to split the data to be transmitted into a number of parallel data streams, each of which modulates a subcarrier. The data rate per subcarrier is only a fraction of conventional single carrier systems having the same throughput. OFDM communication systems naturally mitigate the problem of multipath propagation with its low data rate per subcarrier. In other words, a multipath (frequency-selective) channel is divided into a number of narrowband flat-fading channels. This is one of the biggest advantages of OFDM modulation.

In order to prevent inter-symbol interference (ISI), a guard interval is implemented by means of a cyclic prefix. Thus, each OFDM symbol is preceded by a

periodic extension of the symbol itself. The total OFDM symbol duration is $T_{SYM} = T_{GI} + T$ where T_{GI} is the guard interval and T is the useful symbol duration. When the guard interval is longer than the excess delay of the radio channel, ISI is eliminated.

Pilot tones are often used in OFDM systems for carrier frequency offset and channel estimation refinements. IEEE 802.11a PHY specifies a total of 52 OFDM subcarriers with 48 data subcarriers and 4 pilot subcarriers. Each of the subcarriers is spaced 312.5 kHz apart and a guard interval of 800 ns is added to each symbol making the total symbol duration 4.0 μs.

2.2.2 IEEE 802.11a PHY Frame Structure

As shown in Figure 2.4, a complete PPDU defined in the IEEE 802.11a standard consists of the OFDM PLCP preamble, OFDM PLCP header, PHY service data unit (PSDU), tail bits and pad bits. In the standard, the OFDM PLCP preamble includes two kinds of OFDM training signals with different symbol periods, which are used for synchronization in the receiver. The PLCP header and the following PSDU jointly form the SIGNAL and DATA fields of the PPDU frame. The PLCP header of the PPDU frame is composed of several fields, and the information conveyed in these fields is processed in the receiver to aid the demodulation and delivery of PSDU from the DATA field.

2.2.2.1 PLCP Preamble Field

The main function of the PLCP preamble field is for receiver synchronization, and the structure of the preamble defined in the IEEE 802.11a standard is shown in Figure 2.5. The preamble includes two parts. The first part is composed of 10 repetitions of a short OFDM training signal with a symbol period of 0.8 μs, which is a quarter of the fast Fourier transform (FFT) interval of a normal data OFDM signal, 3.2 μs. The second part of the preamble consists of one cyclic prefix with 1.6 μs and two successive long OFDM training signals with a symbol period 3.2 μs. Note that the length of the cyclic prefix in the second part of the preamble is two times longer than that of a normal data OFDM signal, and the cyclic prefix is a copy of the latter half of the long OFDM training signal. In the following, we will describe the characteristics and functions of the short and long OFDM training signals, respectively.

Short OFDM training signal

A short OFDM training signal consists of 12 subcarriers, which are modulated by the elements of the sequence S, given by

$$
\begin{aligned}
&S_{-26,\,26} = \sqrt{(13/6)} \times \\
&\Big\{ \quad 0,\,0,\quad 1+j,\,0,\,0,\,0,\,-1-j,\,0,\,0,\,0,\,1+j,\,0,\,0,\,0,\,-1-j, \\
&\quad 0,\,0,\,0,\,-1-j,\,0,\,0,\,0,\quad 1+j,\,0,\,0,\,0,\qquad 0,\,0,\,0,\,0,\,-1-j, \\
&\quad 0,\,0,\,0,\,-1-j,\,0,\,0,\,0,\quad 1+j,\,0,\,0,\,0,\;\; 1+j,\,0,\,0,\,0,\quad 1+j, \\
&\quad 0,\,0,\,0,\quad 1+j,\,0,\,0 \Big\}
\end{aligned}
\tag{2.2}
$$

where we number the 53 subcarriers (including dc) from –26 to 26 and the 0-th subcarrir denotes dc. The multiplication by a factor of $\sqrt{(13/6)}$ is to normalize the average power of the resulting OFDM signal, which utilizes 12 out of 52 subcarriers.

From the sequence S in (2.2), the subcarrier numbers chosen by the short training signal are a multiple of 4. It means that the short OFDM training signal has the fundamental frequency of four subcarrier spacings, $4/T_{FFT}$ (where the T_{FFT} is the FFT interval listed in Table 2.2). Hence, the symbol period of the short training signal is $T_{FFT}/4 = 0.8\ \mu s$ and is a quarter smaller than that of the normal data OFDM signal, T_{FFT}. The short OFDM training signals used in the first part of the PLCP preamble field have two purposes. First, the short training signals provide a convenient way of performing automatic gain control (AGC) and frame detection. There are two general methods used to detect the presence of the frame. One is by correlating the received OFDM training signal with its delayed version, and the other is by matched filtering with the training signal. The second purpose for using short training signals is to perform frequency offset estimation and timing synchronization. In the receiver, by using the short OFDM training signals to estimate the frequency offset, we can have the maximum estimation range of two subcarrier spacings. The IEEE 802.11a standard specifies that the maximum frequency offset per user shall be less than ± 20 ppm of the carrier frequency [20]. As the worst case arising between the transmitter and receiver, the frequency offset will be up to 40 ppm of the carrier frequency seen by the receiver. At a carrier frequency of 5.8 GHz, a 40 ppm of carrier frequency offset is approximately equal to a subcarrier spacing, 312.5 kHz. Hence, the range of frequency offset estimation using the short OFDM training signals can support this case well.

Long OFDM training signal

A long OFDM training signal consists of 53 subcarriers (including a zero value at dc), and the subcarriers are modulated by the elements of the sequence L, given by

$$
\begin{aligned}
&L_{-26,\,26} = \\
&\{\ \ 1,\ \ 1,\ -1,\ -1,\ \ 1,\ \ 1,\ -1,\ \ 1,\ -1,\ 1,\ 1,\ \ 1,\ \ 1,\ \ 1,\ \ 1,\ \ 1, \\
&-1,\ -1,\ \ 1,\ \ 1,\ -1,\ \ 1,\ -1,\ \ 1,\ \ 1,\ \ 1,\ 1,\ 0,\ \ 1,\ -1,\ -1,\ \ 1, \\
&\ \ 1,\ -1,\ \ 1,\ -1,\ \ 1,\ -1,\ -1,\ -1,\ -1,\ -1,\ 1,\ 1,\ -1,\ -1,\ \ 1,\ -1, \\
&\ \ 1,\ -1,\ \ 1,\ \ 1,\ \ 1,\ \ 1\ \}
\end{aligned}
\tag{2.3}
$$

In the IEEE 802.11a standard, the long OFDM training signals are also used to evaluate the frequency offset. The maximum range of frequency offset estimation using the long training signals is only half of a subcarrier spacing which is smaller than that by using the short training signals. However, the smaller estimation range the frequency offset estimator has, the more accurate the estimation result we can gain. Hence, we call frequency offset estimation using the long OFDM training signals as the fine frequency offset estimation and that using short OFDM training signals as the coarse frequency offset estimation. In addition, there is another purpose for the long OFDM training signals used in the second part of the PLCP preamble field. Considering a K-subcarrier OFDM system, the relation among the received OFDM signals, the transmitted OFDM signals and the channel effect is given by

$$y_k = x_k \cdot h_k \tag{2.4}$$

for $k = 1, \ldots, K,$ where x_k is the transmitted subsymbol, y_k is the received subsymbol, and h_k is the frequency response of the channel at the kth subcarrier, respectively. Hence, we can use the long OFDM training signals to perform channel estimation by dividing the received subsymbols by the known elements in (2.3). After channel

estimation using the long OFDM training signals, we can use the information of the channel to cancel the channel effect and recover the data subsymbols in the OFDM signals by using the relation described in (2.4).

2.2.2.2 SIGNAL Field and DATA Field

As shown in Figure 2.4, the PLCP header contains the following fields: RATE, LENGTH, a reserved bit, an even parity bit and SERVICE. During the OFDM signal modulation, RATE, LENGTH, the reserved bit and parity bit (with 6 “zero” tail bits appended) constitute a separate single OFDM signal, denoted as SIGNAL. In the transmitter, the SIGNAL field is transmitted with a robust combination of the BPSK modulation and a coding rate of R=1/2. The SEVERICE field of the PLCP header and the PSDU (with 6 “zero” tail bits and pad bits appended) constitute multiple OFDM signals, denoted as DATA. The function of each field in the SIGNAL and DATA fields will be introduced in the following.

SIGNAL field

The SIGNAL field is composed of 24 bits and the bit assignment of each field is illustrated in Figure 2.6. The RATE field occupies the first four bits of the SIGNAL field, and conveys the information about the data rate chosen to transmit the following PSDU. The mapping between the data rate and the content of the RATE field is shown in Table 2.3. By the information from the RATE field, the receiver can determine what type of modulation and what coding rate of the FEC coding are used in PSDU. Bits 5-16 of the SIGNAL field are the LENGTH field, and the information conveyed in this field indicates the number of octets in PSDU, which MAC requests PHY to transmit.

The number of octets in the LENGTH field shall be an unsigned 12-bit integer and has the range from 1 to 4095, and the least significant bit (LSB) shall be transmitted first in time. For the other bits, bit 4 is reversed for future use and bit 17 is a positive parity (even parity) bit for bits 0-16. The last six bits 18-23 constitute the TAIL field of the SIGNAL filed, and all 6 bits are set to zero. The goal of the TAIL field used here is to return the convolutional encoder to the “zero state”. Because the information conveyed in the RATE and LENGTH fields are required for coding the DATA field of the PPDU frame, it is required that these fields can be decoded immediately after the reception of the TAIL field.

DATA field

The DATA field consists of the SERVICE field, PSDU, tail bits and pad bits. In the process of encoding the DATA field into the OFDM signals in the transmitter, all data bits in the DATA field shall be scrambled by a data scrambler. In the receiver, there is a reverse operation performed by a descrambler to recover the data bits. The function of the SERVICE subfield in the DATA field is used to synchronize this descrambler in the receiver. In the DATA field, the SERVICE field occupies first sixteen bits, denoted as bits 0-15, and the bit assignment of the SERVICE field is shown in Figure 2.7. Bits 0-6 of the SERVICE filed are set to zeros and used to synchronize the descrambler in the receiver. The remaining 9 bits (bits 7-15) of the SEVRICE field are reversed for future use and all shall be set to zero. In the DATA field, the tail bits are composed of six bits of “0” and are also used to return the convolutional decoder to the “zero state”. By this procedure, the decoded errors arising in this PPDU frame will not propagate to the next PPDU frame. Hence, we can improve the error probability of the convolutional decoder in the receiver by returning

the convolutional decoder back to “zero state”.

As mentioned, the OFDM system defined in the standard can support eight different data rates. For different data rates chosen to transmit the DATA field, the number of data bits in an OFDM signal, denoted N_{DBPS}, is also different. The relation between N_{DBPS} and data rate is listed in Table 2.1, and the number of the data bits in the DATA field shall be a multiple of N_{DBPS}. To achieve this condition, the pad bits are used to append in the back of the tail bits in the DATA field. The number of pad bits, N_{PAD}, required is computed from the length of PSDU (LENGTH) as follows:

$$N_{SYM} = \text{ceil}\left((16 + 8 \times \text{LENGTH} + 6) / N_{DBPS}\right) \tag{2.5}$$

$$N_{DATA} = N_{SYM} \times N_{DBPS} \tag{2.6}$$

$$N_{PAD} = N_{DATA} - (16 + 8 \times \text{LENGTH} + 6) \tag{2.7}$$

where $\text{ceil}(\cdot)$ is a function that returns the smallest integer value greater than or equal to its argument, N_{SYM} denotes the number of OFDM signals in the DATA field and N_{DATA} is the number of bits in the DATA field. These pad bits are all set to “0” and also shall be scrambled by a data scrambler.

2.3 Summary

In this chapter, we introduce the principles of mandatory DCF mechanism of IEEE 802.11 MAC and OFDM characteristics of IEEE 802.11a PHY. Relying on these understandings, we can further analyze the IEEE 802.11a systems in the later chapters.

(a)

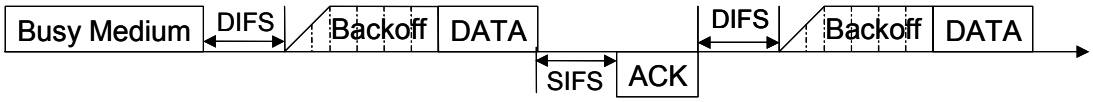

(b)

(c)

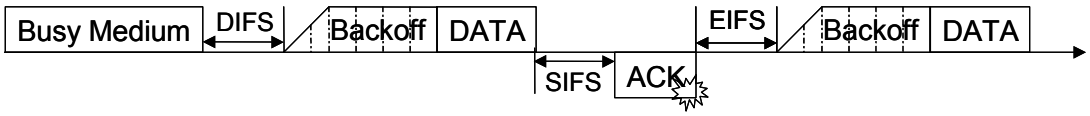

Figure 2.1: Timing of frame transmissions under basic access method (a) Successful frame transmission (b) Frame retransmission due to data frame failure (c) Frame retransmission due to ACK failure

(a)

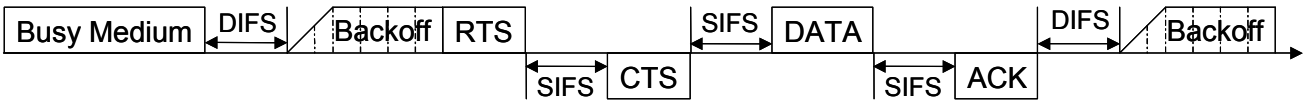

(b)

(c)

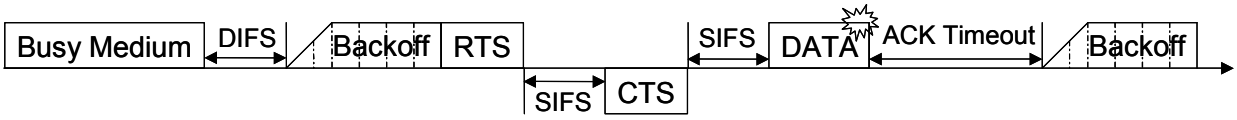

(d)

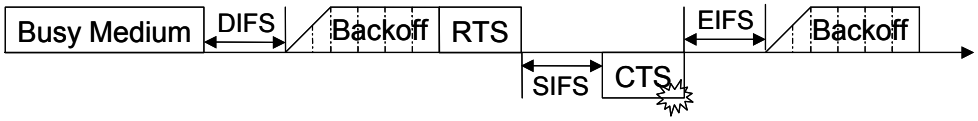

(e)

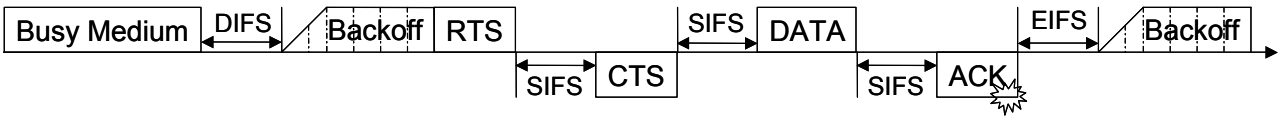

Figure 2.2: Timing of frame transmissions under RTS/CTS access method (a) Successful frame transmission (b) Frame retransmission due to RTS failure (c) Frame retransmission due to data frame failure (d) Frame retransmission due to CTS failure (e) Frame retransmission due to ACK failure

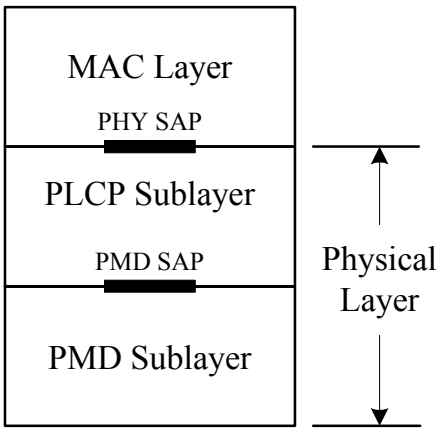

Figure 2.3: Layer and sublayer defined in IEEE 802.11a standard

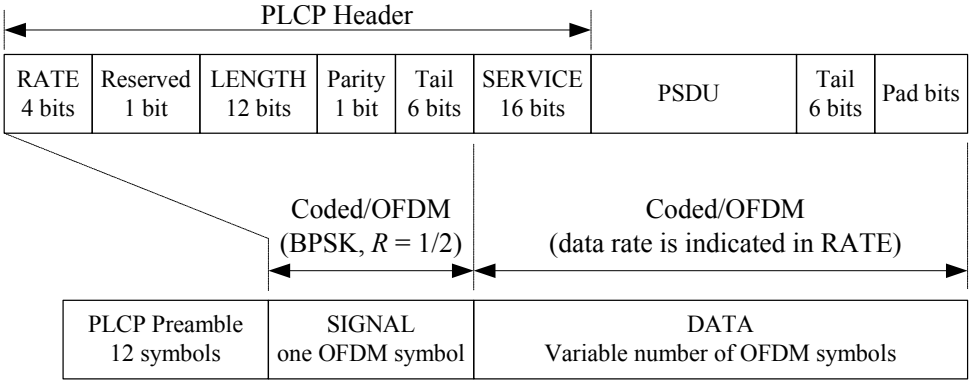

Figure 2.4: PPDU frame format defined in IEEE 802.11a standard

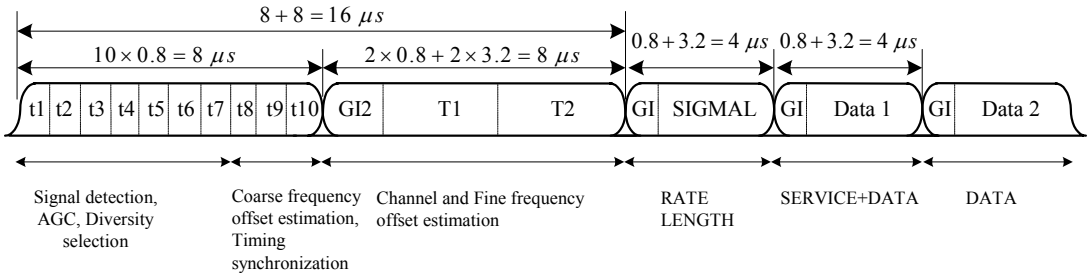

Figure 2.5: Structure of PLCP preamble field defined in IEEE 802.11a standard

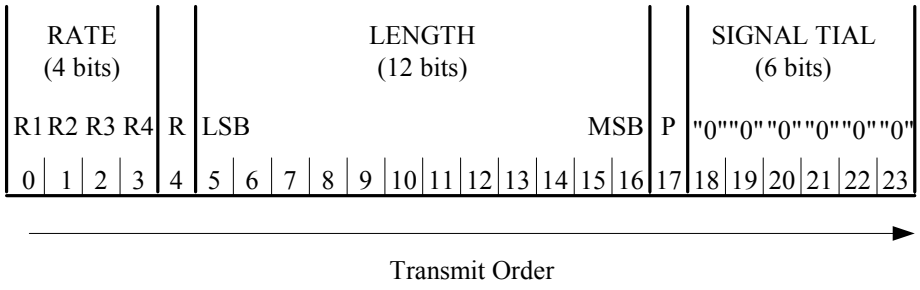

Figure 2.6: Bit assignment in SIGNAL field

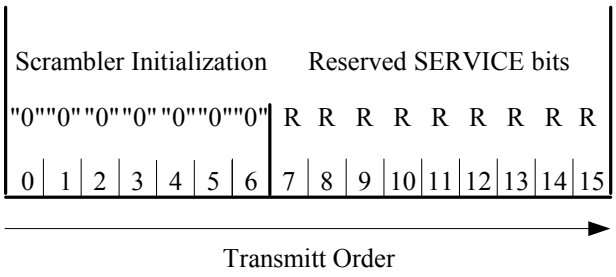

Figure 2.7: Bit assignment in SERVICE field

Table 2.1: Rate-dependent parameters of IEEE 802.11a PHY

Mode	Data rate (Mbits/s)	Modulation	Coding rate (R)	Code bits per subcarrier (N_{BPSC})	Code bits per OFDM symbol (N_{CBPS})	Data bits per OFDM symbol (N_{DBPS})	Data bytes per OFDM symbol (BpS)
1	6	BPSK	1/2	1	48	24	3
2	9	BPSK	3/4	1	48	36	4.5
3	12	QPSK	1/2	2	96	48	6
4	18	QPSK	3/4	2	96	72	9
5	24	16-QAM	1/2	4	192	96	12
6	36	16-QAM	3/4	4	192	144	18
7	48	64-QAM	2/3	6	288	192	24
8	54	64-QAM	3/4	6	288	216	27

Table 2.2: Timing-related parameters of IEEE 802.11a PHY

Parameter	Value
N_{SD}: Number of data subcarriers	48
N_{SP}: Number of pilot subcarriers	4
N_{ST}: Number of subcarriers, total	52 ($N_{SD} + N_{SP}$)
Δ_F: Subcarrier frequency spacing	0.3125 MHz (=20MHz/64)
T_{FFT}: IFFT/FFT period	3.2 μs ($1/\Delta_F$)
T_{Slot}: Slot time	9 μs
T_{SIFS}: SIFS time	16 μs
T_{DIFS}: DIFS time	34 μs ($=T_{SIFS} + 2\times T_{Slot}$)
CWmin: minimum contention window size	15
CWmax: maximum contention window size	1023
$T_{PREAMBLE}$: PLCP preamble duration	16 μs ($T_{SHORT} + T_{LONG}$)
T_{SIGNAL}: Duration of the SIGNAL BPSK-OFDM symbol	4.0 μs ($T_{GI} + T_{FFT}$)
T_{GI}: Guard interval duration	0.8 μs ($T_{FFT}/4$)
T_{GI2}: Training symbol guard interval duration	1.6 μs ($T_{FFT}/2$)
T_{SYM}: Symbol interval	4 μs ($T_{GI} + T_{FFT}$)
T_{SHORT}: Short training sequence duartion	8 μs ($10 \times T_{FFT}/4$)
T_{LONG}: Long training sequence duartion	8 μs ($T_{GI2} + 2 \times T_{FFT}$)

Table 2.3: Contents of RATE field

Rate (Mbps)	R1-R4
6	1101
9	1111
12	0101
18	0111
24	1001
36	1011
48	0001
54	0011

Chapter 3

Link Adaptation for IEEE 802.11a Systems

As mentioned in Section 2.1.2, one of the benefits of the RTS/CTS access method is to increase the system performance by minimizing the amount of time wasted when collisions occur on long data frames. On the other hand, the two additional frames without any payload (RTS and CTS) decrease efficiency. For that reason, the use of the RTS/CTS access method is under the control of the manageable object, RTS_Threshold, which indicates the data length under which the data frames should be sent without RTS/CTS. The data frame size is the only parameter that is used for deciding whether the mechanism is applied [2][3]. But what we are really concerned about is the transmission duration of the data frame not the length. However, the higher the PHY rate, the shorter the transmission time. Therefore, an integrated mechanism, which could consider both the length of the data frame and the used PHY rate, is needed.

In [10], a generic method to analyze the goodput (good throughput, excluding MAC/PHY overheads at MAC layer) performance of the IEEE 802.11a system is presented. Utilizing and extending this goodput analysis, we propose an link adaptation (LA) algorithm which could not only select the transmission rate but also

the MAC mechanism (the basic access method or RTS/CTS access method). In this LA algorithm, besides data payload length, we consider other parameters like the wireless channel condition and number of contending stations to select the best combination of the MAC mechanism and PHY mode.

In this chapter, we will analyze the collision probability of the IEEE 802.11a system in Section 3.1. Some detailed MAC and PHY characteristics including MAC/PHY overheads and error performance of IEEE 802.11a PHY modes will be introduced in Section 3.2 and 3.3, respectively. Section 3.4 shows the analysis of effective goodput of the 802.11a system. Based on the results obtained in Section3.4, a LA algorithm is proposed in Section 3.5 and evaluated in Section 3.6.

3.1 Collision Probability

In [2][21], Markov process is used to analyze the performance of the 802.11 system and show that the Markov chain analysis method is suitable for examining the performance of the IEEE 802.11 system, which captures the effect of the CW value and binary slotted exponential backoff procedure used by DCF in IEEE 802.11. The Markov model in [22] can be regarded as an extension of the model in [2][21], which takes the retransmission limit of MAC frames into account, therefore a more exact model is proposed. With this Markov model, the behavior of a station is examined, which we use to get the collision probability p that a transmitted frame collides with another. We put the obtained collision probability in the 802.11a system to the later use for computing the effective goodput.

In this section, the assumptions necessary for the presented analytical framework are as follows:

1. We ignore the effect of frame errors due to bit errors introduced by channel noise since the effect of frame errors is small (shown in later section). Therefore, frames are received in error only when they encounter collisions due to other simultaneous transmissions.
2. No hidden stations and propagation delays are considered.
3. The network consists of a fixed number of contending stations n and every station always has a frame available for transmission (saturated conditions). Moreover being all frames consecutive, each frame needs to wait for a random backoff time before transmitting.
4. The main approximation is that the collision probability of a transmitted frame is constant and independent of the number of retransmission that this frame has experienced in the past.

Let $b(t)$ be the stochastic process representing the backoff window size for a given station at slot time t. A discrete and integer time scale is adopted: t and $t+1$ correspond to the beginning of two consecutive slot times, and the backoff counter of each station decrements at the beginning of each slot time. Let $s(t)$ be the stochastic process representing the backoff stage (0,…,m) of the station at time t. According to the above assumptions, the bi-dimensional process $\{s(t),\ b(t)\}$ is possible to be modeled with the discrete-time Markov chain, which is shown in Figure 3.1.

In IEEE 802.11a PHY, $CWmin$ and $CWmax$ equal to 15 and 1023, respectively (as shown in Table 2.2). Therefore we have

$$\begin{cases} W_i = 2^i W & i \le m' \\ W_i = 2^{m'} W & i > m' \end{cases} \tag{3.1}$$

where $i \in (0,m)$ is called backoff stage, W=($CWmin$+1), and $2^{m'}W$=($CWmax$+1), so for IEEE 802.11a PHY, we have m' = 6. We use m to represent maximum backoff stage. As specified in IEEE 802.11, this value could be larger than m' and the CW value will be hold after that, which is shown in equation (3.1). In fact, m is the $ShortRetryLimit$ and equal to 7 according to the standard described in Section 2.1.1. In this Markov chain, the only non-null one-step transition probabilities are

$$\begin{cases} P\{i,k \mid i,k+1\} = 1 & k \in [0,W_i - 2],\ i \in [0,m] \\ P\{0,k \mid i,0\} = (1-p)/W_0 & k \in [0,W_0 - 1],\ i \in [0,m-1] \\ P\{i,k \mid i-1,0\} = p/W_i & k \in [0,W_i - 1],\ i \in [1,m] \\ P\{0,k \mid m,0\} = 1/W_0 & k \in [0,W_0 - 1] \end{cases} \tag{3.2}$$

where we adopt the short notation:

$$P\{i_1,k_1 \mid i_0,k_0\} = P\{s(t+1) = i_1, b(t+1) = k_1 \mid s(t) = i_0, b(t) = k_0\} \tag{3.3}$$

These transition probabilities account, respectively, for: i) the decrements of the backoff timer; ii) after a successful transmission, the backoff timer of the new frame starts from the backoff stage 0, and thus the backoff is initially uniformly chosen in the range ($0, W_0$-1); iii) when an unsuccessful transmission occurs at backoff stage i-1, the backoff stage increases, and the new initial backoff value is uniformly chosen in the range ($0, W_i$-1); iv) at the maximum backoff stage, the CW value will be reset if the transmission is unsuccessful or restart for a new frame if the transmission is successful.

Let $b_{i,k} = \lim_{t\to\infty} P\{s(t) = i, b(t) = k\},\ i \in (0,m),\ k \in (0, W_i - 1)$ be the stationary distribution of the Markov chain. First note that

$$b_{i-1,0} \cdot p = b_{i,0} \qquad 0 < i \le m \tag{3.4}$$

then

$$b_{i,0} = p^i b_{0,0} \qquad 0 < i \le m \tag{3.5}$$

Since the chain is regular, so for each $k \in \left(0, W_i - 1\right)$, it is

$$b_{i,k} = \frac{W_i - k}{W_i} \begin{cases} (1-p)\sum_{j=0}^{m-1} b_{j,0} + b_{m,0} & i = 0 \\ p b_{i-1,0} & 0 < i \le m \end{cases} \tag{3.6}$$

With (3.5) and transition in the chain, equation (3.6) can be simplified as

$$b_{i,k} = \frac{W_i - k}{W_i} b_{i,0} \qquad 0 \le i \le m \tag{3.7}$$

Thus, by (3.5) and (3.7), all the value $b_{i,k}$ are expressed as functions of the value $b_{0,0}$ and collision probability p. Impose the normalization condition for the stationary distribution as follows.

$$1 = \sum_{i=0}^{m} \sum_{k=0}^{W_i - 1} b_{i,k} = \sum_{i=0}^{m} b_{i,0} \sum_{k=0}^{W_i - 1} \frac{W_i - k}{W_i} = \sum_{i=0}^{m} b_{i,0} \frac{W_i + 1}{2} \tag{3.8}$$

From (3.1), (3.7), and (3.8), $b_{0,0}$ is finally determined.

$$b_{0,0} = \begin{cases} \dfrac{2(1-2p)(1-p)}{W\left(1-(2p)^{m+1}\right)(1-p) + (1-2p)\left(1-p^{m+1}\right)} & m \le m' \\ \dfrac{2(1-2p)(1-p)}{W\left(1-(2p)^{m'+1}\right)(1-p) + (1-2p)\left(1-p^{m+1}\right) + W 2^{m'} p^{m'+1}(1-2p)\left(1-p^{m-m'}\right)} & m > m' \end{cases} \tag{3.9}$$

As any transmission occurs when the backoff counter is equal to zero, regardless of the backoff stage, the probability τ that a station transmits in a randomly chosen slot time can be expressed as

$$\tau = \sum_{i=0}^{m} b_{i,0} = \frac{1 - p^{m+1}}{1 - p} b_{0,0} \tag{3.10}$$

where $b_{0,0}$ can be obtained from equation (3.9).

However, in general, τ depends on the collision probability p, which is still

unknown. To find the value of p, it is sufficient to note that the probability p that a transmitted packet encounters a collision is the probability that, in a time slot, at least one of the n-1 remaining stations transmit. The fundamental independence assumption given above implies that each transmission sees the system in the same state, i.e., in steady state. At steady state, each remaining station transmits a frame with probability τ. This yields

$$p = 1 - (1 - \tau)^{n-1} \tag{3.11}$$

Therefore, equations (3.10) and (3.11) represent a nonlinear system with the two unknown variables τ and p, which can be solved by the numerical technique. It is easy to prove that this system has a unique solution. In fact, inverting (3.11), we can obtain $\tau^*(p) = 1 - (1-p)^{1/(n-1)}$. This is a continuous and monotone increasing function in the range $p \in (0,1)$, that starts from $\tau^*(0) = 0$ and grows up to $\tau^*(1) = 1$. Equation $\tau(p)$ defined by (3.10) is also continuous in the range $p \in (0,1)$. Moreover, $\tau(p)$ is trivially shown to be a monotone decreasing function. Uniqueness of the solution is now proven noting that $\tau(0) > \tau^*(0)$ and $\tau(1) < \tau^*(1)$. Figure 3.2 shows the numerical solutions of both equations with varying values of n, the number of contending stations. For each value of n, the solution yields a unique value for the collision probability p that we will utilize to compute the effective goodput in the later section. The value of the collision probability is sensitive to the number of stations, n. This is shown in Figure 3.2 and Figure 3.3 in which the value of p increases as we increase the number of stations, n. This is an expected result because the number of stations increases, there is more contention among all the stations.

3.2 MAC/PHY Layer Overheads

As shown in Figure 3.4(a), in IEEE 802.11 MAC, each MAC data frame, or MPDU, consists of the following components: the MAC header, variable-length information frame body (MAC service data unit, MSDU), and FCS. The MAC overhead due to the MAC header and the FCS is 28 octets in total. Actually, an additional field of Address 4 is used only for the wireless AP-to-AP communication, which is not common, and hence we assume that is not used. Besides, the information frame body (data payload) can be up to 2312 if encryption is used, but we assume that encryption is not used. Figure 3.4(b)~(d) illustrate the frame formats of the RTS, CTS, and ACK frames, which are 20, 14, and 14 octets long respectively.

Review Section 2.2, during the transmission, a PLCP preamble and a PLCP header are added to an MPDU to create a PPDU. The PPDU format of the IEEE 802.11a PHY is shown in Figure 2.4, which includes the PLCP preamble, PLCP header, PSDU (i.e. MPDU conveyed from MAC), tail bits, and pad bits (if necessary). The PLCP preamble field, with the duration of $T_{PREAMBLE}$, is composed of 10 repetitions of a short training signal (0.8 μs) and two repetitions of a long training signal (4 μs). The PLCP header, except the SERVICE field, with the duration of T_{SIGNAL}, constitutes a single OFDM symbol, which is transmitted with the BPSK modulation and rate-1/2 convolutional coding. The six zero tail bits are used to return the convolutional decoder to the zero state and the pad bits are used to make the resulting bit string into a multiple of OFDM symbols. Each OFDM symbol interval, denoted by T_{SYM}, is 4 μs. The 16-bit SERVICE field of the PLCP header and MPDU (along with six tail bits and pad bits), represented by DATA, are transmitted at the data rate specified in the RATE field. Table 2.2 lists the related characteristics for IEEE 802.11a PHY.

Note that, while the data frame MPDUs can be transmitted at any supported data rate, all the control frames, including the RTS, CTS, and ACK frames, have to be transmitted at one of the rates in the BSS basic rate set so that they can be understood by all the stations in the same network. BSS basic rate set data rates are preset for all the stations in BSS. {6 Mbps, 12Mbps, 24Mbps} is the set of the IEEE 802.11a mandatory data rates, and it will be assumed to be the BSS basic rate set in our example and simulations. In addition, the RTS and CTS frame will be transmitted at the lowest rate in the BSS basic rate set (6Mbps) while the ACK frame transmitted at the highest rate in the BSS basic rate set that is less than or equal to the rate of the data frame it is acknowledging. For example, if a data frame is transmitted at the rate of 18 Mbps, the corresponding ACK frame will be transmitted at the rate of 12 Mbps.

Based on the above descriptions, to transmit a frame with an l-octet data payload over IEEE 802.11a PHY using the PHY mode m, the transmission duration is

$$\begin{aligned} T_{data}(l,m) &= T_{PREAMBLE} + T_{SIGNAL} + \left\lceil \frac{28 + (16+6)/8 + l}{BpS(m)} \right\rceil \cdot T_{SYM} \\ &= 20\mu s + \left\lceil \frac{30.75 + l}{BpS(m)} \right\rceil \cdot 4\mu s \end{aligned} \tag{3.12}$$

Note that the Bytes-per-Symbol information for the PHY mode m, $BpS(m)$, is given in Table 2.1. Similarly, the transmission duration for a RTS frame and a CTS frame are

$$\begin{aligned} T_{rts} &= T_{PREAMBLE} + T_{SIGNAL} + \left\lceil \frac{20 + (16+6)/8}{BpS(1)} \right\rceil \cdot T_{SYM} \\ &= 20\mu s + \left\lceil \frac{22.75}{3} \right\rceil \cdot 4\mu s = 52\mu s \end{aligned} \tag{3.13}$$

and

$$T_{cts} = T_{PREAMBLE} + T_{SIGNAL} + \left\lceil \frac{14 + (16+6)/8}{BpS(1)} \right\rceil \cdot T_{SYM}$$
$$= 20\mu s + \left\lceil \frac{16.75}{3} \right\rceil \cdot 4\mu s = 44\mu s \tag{3.14}$$

respectively. Note that the transmission rate of RTS and CTS is the lowest BSS basic rate, 6Mbps, i.e. PHY mode 1. And the transmission duration for an ACK frame using the PHY mode m' is

$$T_{ack}(m') = T_{PREAMBLE} + T_{SIGNAL} + \left\lceil \frac{14 + (16+6)/8}{BpS(m')} \right\rceil \cdot T_{SYM}$$
$$= 20\mu s + \left\lceil \frac{16.75}{BpS(m')} \right\rceil \cdot 4\mu s \tag{3.15}$$

The relation between m and m' is discussed above.

3.3 Error Performance of PHY Modes

3.3.1 Bit Error Probability

The symbol error probability (SER) for an M-ary (M=4, 16, 64) QAM with the average received SNR per symbol, γ, can be calculated by [23]

$$P_M(\gamma) = 1 - \left[1 - P_{\sqrt{M}}(\gamma)\right]^2 \tag{3.16}$$

where

$$P_{\sqrt{M}}(\gamma) = 2 \cdot \left(1 - \frac{1}{\sqrt{M}}\right) \cdot Q\left(\sqrt{\frac{3}{M-1} \cdot \gamma}\right) \tag{3.17}$$

is the SER for the $\sqrt{M}-$ary pulse amplitude modulation (PAM).

And

$$\gamma = \frac{E\left\{\left|x_k\right|^2\right\} \cdot \frac{\sum_{k=1}^{N_c\_data} \left|h_k\right|^2}{N_c\_data}}{N_0} = \frac{E_s \cdot \sum_{k=1}^{N_c\_data} \left|h_k\right|^2}{N_0 \cdot N_c\_data} \tag{3.18}$$

The Q-function is defined as

$$Q(x) = \int_x^\infty \frac{1}{\sqrt{2\pi}} e^{-y^2/2} dy \tag{3.19}$$

With a Gray coding, the bit error probability (BER) for an *M*-ary QAM can be approximated by

$$P_b^{(M)}(\gamma) \approx \frac{1}{\log_2 M} \cdot P_M(\gamma) \tag{3.20}$$

Note that the 4-ary QAM and QPSK modulation are identical. For the BPSK modulation, BER is the same as SER, which is given by

$$P_b^{(2)}(\gamma) = P_2(\gamma) = Q\left(\sqrt{2\gamma}\right) \tag{3.21}$$

Obviously, the error performance of a modulation scheme varies with different received SNR values.

3.3.2 Frame Error Probability

In [24], an upper bound was given on the frame error probability under the assumption of binary convolutional coding and hard-decision Viterbi decoding with independent errors at the channel input. For an *l*-octet long frame to be transmitted using the PHY mode m, this bound is

$$P_e^m(l,\gamma) \le 1 - \left[1 - P_u^m(\gamma)\right]^{8l} \tag{3.22}$$

where the union bound $P_u^m(\gamma)$ of the first-event error probability is given by

$$P_u^m(\gamma) = \sum_{d=d_{free}}^{\infty} a_d \cdot P_d(\gamma) \tag{3.23}$$

where d_{free} is the free distance of the convolutional code selected in the PHY mode m, a_d is the total number of error events of weight d, and $P_d(\gamma)$ is the probability that an incorrect path at the distance d from the correct path being chosen by the Viterbi decoder. When the hard-decision decoding is applied, $P_d(\gamma)$ is given by

$$P_d(\gamma) = \begin{cases} \sum_{k=(d+1)/2}^{d} \binom{d}{k} \cdot \rho^k \cdot (1-\rho)^{d-k}, & \text{if } d \text{ is odd} \\ \frac{1}{2} \cdot \rho^{d/2} \cdot (1-\rho)^{d/2} + \sum_{k=d/2+1}^{d} \binom{d}{k} \cdot \rho^k \cdot (1-\rho)^{d-k}, & \text{if } d \text{ is even} \end{cases} \tag{3.24}$$

where ρ is BER for the modulation scheme selected in the PHY mode m and given by (3.20) or (3.21). The value of a_d can be obtained either from the transfer function or by a numerical search [25]. Here, we use the a_d coefficients provided in [26]. Figure 3.5 shows the upper bound BER performance, $P_u^m(\gamma)$, of the different IEEE 802.11a PHY modes versus the average received SNR, γ.

Consider the RTS/CTS access method, the only frame will suffer the collision is the RTS frame. Thus, $P_{e,rts}(\gamma, n)$, the RTS frame error probability, can be calculated by

$$\begin{aligned} P_{e,rts}(\gamma, n) &= 1 - \left[1 - P_{collision}(n)\right] \cdot \left[1 - P_e^1\left(24/8 + 20 + (16+6)/8, \gamma\right)\right] \\ &= 1 - \left[1 - P_{collision}(n)\right] \cdot \left[1 - P_e^1(25.75, \gamma)\right] \end{aligned} \tag{3.25}$$

where n represent the number of contending stations. Note that the term $P_e^1\left(24/8 + 20 + (16+6)/8, \gamma\right)$ represents the PCLP SIGNAL field (24-bit long) plus the length of the RTS frame format (20-octet long) along with the 16-bit SERVICE field, six tail bits, and pad bits, which are transmitted with the BPSK modulation and rate-1/2 convolutional coding, i.e. PHY mode 1.

On the other hand, $P_{e,cts}(\gamma)$, the CTS frame error probability, $P_{e,data}(l,\gamma,m)$, the data frame error probability, and $P_{e,ack}(\gamma,m')$, the ACK frame error probability are shown below

$$\begin{aligned} P_{e,cts}(\gamma) &= 1-\left[1-P_e^1\left(24/8+14+(16+6)/8,\gamma\right)\right] \\ &= 1-\left[1-P_e^1(19.75,\gamma)\right] \end{aligned} \tag{3.26}$$

$$\begin{aligned} P_{e,data}(l,\gamma,m) &= 1-\left[1-P_e^1(24/8,\gamma)\right]\cdot\left[1-P_e^m\left(28+(16+6)/8+l,\gamma\right)\right] \\ &= 1-\left[1-P_e^1(3,\gamma)\right]\cdot\left[1-P_e^m(30.75+l,\gamma)\right] \end{aligned} \tag{3.27}$$

$$\begin{aligned} P_{e.ack}(\gamma,m') &= 1-\left[1-P_e^1\left(24/8,\gamma\right)\right]\cdot\left[1-P_e^{m'}\left(14+(16+6)/8,\gamma\right)\right] \\ &= 1-\left[1-P_e^1(3,\gamma)\right]\cdot\left[1-P_e^{m'}(16.75,\gamma)\right] \end{aligned} \tag{3.28}$$

$P_e^1(\cdot)$, $P_e^m(\cdot)$, and $P_e^{m'}(\cdot)$ are calculated by (3.22).

3.4 Effective Goodput Computation

In this section, we focus our analysis on the effective goodput of the RTS/CTS access method. Our objective is to calculate the maximum throughput achievable with the IEEE 802.11a WLAN at the MAC layer for a given SNR by taking into consideration of the MAC, PHY, and retransmission overheads. In our analysis, we make following assumptions: i) the transmitter generates, at an infinite rate, *l*-octet long data payload (MSDU); ii) the MSDU is not fragmented; iii) the propagation delays are neglected; iv) the constant wireless channel condition throughout the entire frame delivery period. After a station makes the PHY mode selection and starts transmitting, the selected PHY mode will be used for all the potential retransmissions. In brief, a frame with *l*-octet data payload is to be transmitted using the PHY mode m

over the wireless channel with condition γ. Let m' denote the PHY mode used for the corresponding ACK frame transmission and it is determined based on m according to the rule specified in Section 3.2.

To simplify the analysis, we separate the transmission phases of the RTS/CTS access method into two stages: i) channel reservation ii) data transmission. The first stage, channel reservation, includes the DIFS deferral phase, backoff phase, RTS transmission phase, SIFS deferral phase, CTS transmission phase, and SIFS deferral phase. The remained phases belong to the data transmission stage. Now, let's consider the entire delivery progress of the frame transmission. Since the maximum numbers of transmission attempt to deliver the RTS frame and the data frame are specified by $ShortRetryLimit$, denoted as n_s, and $LongRetryLimit$, denoted as n_b, respectively. Recalling Section 2.1.1, every station maintains an SSRC as well as an SLRC. Whenever a CTS frame is received in response to the RTS frame, the SSRC is reset to 0. On the other hand, SLRC is reset to 0 when an ACK is received in response to a data frame. That is to say two counters are independent to each other. An example will make it clearer. Let n_s be 7 and n_l be 4. At beginning, we send the RTS frame but unfortunately it fails, i.e. it fails at the channel reservation stage, for first 6 times. At the 7th attempt, it succeeds. So there are 7 retries in total so far. Now the data frame is sent afterwards, but the transmission fails at the data transmission stage. Then one retry count for the data frame is consumed, i.e. there are 3 more left. Again, the RTS frame is sent, and it will get 7 more chances. Therefore, for a single data frame, there may be totally 28 (7×4) RTS frames and 4 data frames sent in the transmission progress in the worst-case scenario. We illustrate all discussions above with Figure 3.6. $P_{succ,ch}(\gamma, n)$ stands for the probability of a successful channel reservation within the

retry limit and it can be calculated by

$$P_{succ,ch}(\gamma,n) = 1 - \left[1 - P_{s,xmit,ch}(\gamma,n)\right]^{n_s} \tag{3.29}$$

where

$$P_{s,xmit,ch}(\gamma,n) = \left[1 - P_{e,rts}(\gamma,n)\right] \cdot \left[1 - P_{e,cts}(\gamma)\right] \tag{3.30}$$

is the probability of a successful channel reservation. $P_{s,xmit,data}(\gamma,n)$ represents the probability of a successful data transmission and it can be computed by

$$P_{s,xmit,data}(l,\gamma,m) = \left[1 - P_{e,data}(l,\gamma,m)\right] \cdot \left[1 - P_{e,ack}(\gamma,m)\right] \tag{3.31}$$

By referring to Figure 2.2(a), a successful channel reservation duration is equal to a backoff delay, plus the RTS transmission time, plus an SIFS time, plus the CTS transmission time, and plus an SIFS time. However, whenever the channel reservation fails, the station has to wait for a CTS_Timeout period or an EIFS interval, and then execute a backoff procedure before the retransmission (see Figure 2.2(b) and (d)). According to the IEEE 802.11 MAC standard, an EIFS interval is equal to an SIFS time plus a DIFS time plus the ACK transmission time at the most robust 6 Mbps and a CTS_Timeout is equal to an SIFS time plus a CTS transmission time plus a Slot_Time. Therefore, the average transmission duration of the channel reservation can be calculated by

$$\begin{aligned} D_{succ,ch}(\gamma,n) = \sum_{k=1}^{n_s} P_{ch}[k \mid succ](\gamma,n) \cdot \\ \left\{ \begin{aligned} &\overline{T}_{bkoff}(1) + T_{rts} + \sum_{i=2}^{k} \left[\overline{D}_{wait,ch}(\gamma,n) + \overline{T}_{bkoff}(i) + T_{rts}\right] \\ &+ T_{SIFS} + T_{cts} + T_{SIFS} \end{aligned} \right\} \end{aligned} \tag{3.32}$$

where $P_{ch}[k \mid succ](\gamma,n)$ is the conditional probability that the channel is successfully reserved at the kth transmission attempt. It can be computed by

$$P_{ch}[k \mid succ](\gamma, n) = \frac{P_{s,xmit,ch}(\gamma, n) \cdot \left[1 - P_{s,xmit,ch}(\gamma, n)\right]^{k-1}}{P_{succ,ch}(\gamma, n)} \tag{3.33}$$

$\overline{T}_{bkoff}(i)$ is the average backoff interval before the ith transmission attempt or, equivalently, the $(i$ -1)th retransmission attempt. It can be calculated by

$$\overline{T}_{bkoff}(i) = \frac{\min\left[2^{i-1} \cdot \left(CWmin + 1\right) - 1, CWmax\right]}{2} \cdot Slot\_Time \tag{3.34}$$

And $\overline{D}_{wait,ch}(\gamma, n)$ is the average waiting time before the next attempt. It can be calculated by

$$\begin{aligned} \overline{D}_{wait,ch}(\gamma, n) = & \frac{P_{e,data}(\gamma, n)}{1 - P_{s,xmit,ch}(\gamma, n)} \cdot \left(T_{SIFS} + T_{cts} + Slot\_Time\right) \\ & + \frac{\left[1 - P_{e,rts}(\gamma, n)\right] \cdot P_{e,cts}(\gamma)}{1 - P_{s,xmit,ch}(\gamma, n)} \cdot \begin{bmatrix} T_{SIFS} + T_{cts} + T_{SIFS} \\ + T_{ack}(1) + T_{DIFS} \end{bmatrix} \end{aligned} \tag{3.35}$$

On the other hand, the average time wasted in attempting reservation of the channel n_s times in error is given by

$$D_{fail,ch}(\gamma, n) = \sum_{i=1}^{n_s} \left[\overline{T}_{bkoff}(i) + T_{rts} + \overline{D}_{wait,ch}(\gamma, n)\right] \tag{3.36}$$

We have discussed the average duration the channel reservation stage takes no matter it succeeds or not. Using this statistics, we can compute the duration for a data frame transmitted using the RTS/CTS access method. By referring to Figure 3.6, the probability of the successful frame transmission within the retry limit is

$$\begin{aligned} P_{succ}(l, \gamma, m, n) = & P_{succ,ch}(\gamma, n) \cdot P_{s,xmit,data}(l, \gamma, m) \cdot \\ & \left\{ \sum_{i=0}^{n_l - 1} \left\{ P_{succ,ch}(\gamma, n) \cdot \left[1 - P_{s,xmit,data}(l, \gamma, m)\right] \right\}^i \right\} \end{aligned} \tag{3.37}$$

A successful exchange of the frame transmission must complete both channel reservation and data transmission stages. Therefore, the overall duration of the frame transmission is equal to a channel reservation duration, plus the data transmission

duration which include the data transmission time, plus an SIFS time, plus the ACK transmission time, and plus a DIFS time. Once the data transmission fails, the station has to wait for an ACK_Timeout period or an EIFS interval, and then perform another channel reservation again (see Figure 2.2(c) and (e)). Therefore, the average transmission duration of the whole frame transmission can be calculated by

$$D_{succ}(l,\gamma,m,n) = \sum_{k=1}^{n_l} P[k \mid succ](l,\gamma,m,n) \cdot \begin{Bmatrix} D_{succ,ch}(\gamma,n) + T_{data}(l,m) \\ +\sum_{i=2}^{k}\left[\overline{D}_{wait,data}(l,\gamma,m) + D_{succ,ch}(\gamma,n) + T_{data}(l,m)\right] \\ +T_{SIFS} + T_{ack}(m') + T_{DIFS} \end{Bmatrix} \quad (3.38)$$

where $P[k \mid succ](l,\gamma,m,n)$ is the conditional probability that the data is successfully transmitted at the kth attempt and it can be computed by

$$P[k \mid succ](l,\gamma,m,n) = \frac{P_{succ,ch}(\gamma,n)^k \cdot P_{s,xmit,data}(l,\gamma,m) \cdot \left[1 - P_{s,xmit,data}(l,\gamma,m)\right]^{k-1}}{P_{succ}(l,\gamma,m,n)} \quad (3.39)$$

$D_{succ,ch}(\gamma,n)$ is given by (3.32) and the average waiting time before the next attempt, $\overline{D}_{wait,data}(l,\gamma,m)$, can be computed by

$$\begin{aligned} \overline{D}_{wait,data}(l,\gamma,m) = {} & \frac{P_{e,data}(l,\gamma,m)}{1 - P_{s,xmit,data}(l,\gamma,m)} \cdot \left(T_{SIFS} + T_{ack}(m') + Slot\_Time\right) \\ & + \frac{\left[1 - P_{e,data}(l,\gamma,m)\right] \cdot P_{e,ack}(\gamma,m)}{1 - P_{s,xmit,data}(l,\gamma,m)} \cdot \begin{bmatrix} T_{SIFS} + T_{ack}(m') \\ +T_{SIFS} + T_{ack}(1) \\ +T_{DIFS} \end{bmatrix} \end{aligned} \quad (3.40)$$

On the other hand, the average time wasted in attempting transmission of the data frame is given by

$$
\begin{aligned}
&D_{fail}(l,\gamma,m,n)\\
&=\frac{1-P_{succ,ch}(\gamma,n)}{1-P_{succ}(l,\gamma,m,n)}\cdot D_{fail,ch}(\gamma,n)\\
&+\frac{P_{succ,ch}(\gamma,n)\cdot\left[1-P_{s,xmit,data}(l,\gamma,m)\right]\cdot\left[1-P_{succ,ch}(\gamma,n)\right]}{1-P_{succ}(l,\gamma,m,n)}\\
&\quad\cdot\left[D_{succ,ch}(\gamma,n)+T_{data}(l,m)+\overline{D}_{wait,data}(l,\gamma,m)+D_{fail,ch}(\gamma,n)\right]\\
&+\frac{\left\{P_{succ,ch}(\gamma,n)\cdot\left[1-P_{s,xmit,data}(l,\gamma,m)\right]\right\}^2\cdot\left[1-P_{succ,ch}(\gamma,n)\right]}{1-P_{succ}(l,\gamma,m,n)}\\
&\quad\cdot\left[2D_{succ,ch}(\gamma,n)+2T_{data}(l,m)+2\overline{D}_{wait,data}(l,s,m)+D_{fail,ch}(s,n)\right]\\
&+\frac{\left\{P_{succ,ch}(\gamma,n)\cdot\left[1-P_{s,xmit,data}(l,\gamma,m)\right]\right\}^3\cdot\left[1-P_{succ,ch}(\gamma,n)\right]}{1-P_{succ}(l,\gamma,m,n)}\\
&\quad\cdot\left[3D_{succ,ch}(\gamma,n)+3T_{data}(l,m)+3\overline{D}_{wait,data}(l,\gamma,m)+D_{fail,ch}(\gamma,n)\right]\\
&+\frac{\left\{P_{succ,ch}(\gamma,n)\cdot\left[1-P_{s,xmit,data}(l,\gamma,m)\right]\right\}^4}{1-P_{succ}(l,\gamma,m,n)}\cdot\begin{bmatrix}4D_{succ,ch}(\gamma,n)+4T_{data}(l,m)\\+4\overline{D}_{wait,data}(l,\gamma,m)\end{bmatrix}
\end{aligned}
\tag{3.41}
$$

The expected effective goodput can then be calculated by

$$
\begin{aligned}
g(l,\gamma,m,n)&=\frac{l}{\sum_{k=0}^{\infty}\left\{\begin{matrix}\left[1-P_{succ}(l,\gamma,m,n)\right]^k\cdot P_{succ}(l,\gamma,m,n)\cdot\\\left(k\cdot D_{fail}(l,\gamma,m,n)+D_{succ}(l,\gamma,m,n)\right)\end{matrix}\right\}}\\
&=\frac{l}{\frac{1-P_{succ}(l,\gamma,m,n)}{P_{succ}(l,\gamma,m,n)}\cdot D_{fail}(l,\gamma,m,n)+D_{succ}(l,\gamma,m,n)}\\
&=\frac{P_{succ}(l,\gamma,m,n)\cdot l}{\left[1-P_{succ}(l,\gamma,m,n)\right]\cdot D_{fail}(l,\gamma,m,n)+P_{succ}(l,\gamma,m,n)\cdot D_{succ}(l,\gamma,m,n)}\\
&=\frac{E[data](l,\gamma,m,n)}{E\left[D_{data}\right](l,\gamma,m,n)}
\end{aligned}
\tag{3.42}
$$

which is based on the fact that, with probability $\left[1-P_{succ}(l,\gamma,m,n)\right]^k\cdot P_{succ}(l,\gamma,m,n)$, there is a successful data frame delivery within the retry limit after dropping the previous k frames. It can also be interpreted as follows: the expected effective goodput is equal to the ratio of the expected delivery data payload to the expected transmission time. Note that, under the constraint of the

frame retry limit, the successfully delivered data payload is no longer a fixed value of l. It is actually a two-value random variable and can take the value of l if delivery succeeds, with probability $P_{succ}(l,\gamma,m,n)$, or 0 if delivery fails. So, $E[data](l,\gamma,m,n) = P_{succ}(l,\gamma,m,n)\cdot l$ is the expected data payload. Similarly, $E\left[D_{data}\right](l,\gamma,m,n)$ is the expected transmission time spent on the frame delivery attempt, irrespectively of whether it is successful or not.

3.5 Link Adaptation Scheme

Note that the higher the PHY mode that are used ($m\uparrow$), the shorter the transmission time will be, but the less likely the delivery will succeed within the frame retry limit ($P_{succ}(l,\gamma,m,n)\downarrow$). So, for any given wireless channel condition, there exists a corresponding PHY mode that maximizes the expected effective goodput. Such a PHY mode is called the best transmission strategy for data frame delivery under the given wireless channel condition. Therefore, an LA algorithm for improving the goodput performance of the IEEE 802.11a WLAN is needed. Its principle is to improve the efficiency of a system by adapting the modulation scheme to the current link condition.

Using the IEEE 802.11a PHY parameters listed in Table 2.2 in the equations derived above, Figure 3.7(a) and (b) show the numerical results of the effective goodput, according to the goodput analysis of different PHY modes with the MSDU size of 200 octets and 2,000 octets in the network consisting of five contending stations, respectively. As expected, the higher rate PHY mode results in better goodput performance in the high SNR range, while the lower rate PHY mode results in better

goodput performance in the low SNR range. One interesting observation is that the PHY mode 3 (QPSK modulation with rate-1/2 coding) always achieves better effective goodput than PHY mode 2 (BPSK modulation with rate-3/4 coding) under all SNR conditions for both frame sizes. The reason for this is that, although QPSK has a higher BER compared to BPSK, the better performance of the rate-1/2 convolutional code compared to rate-3/4 convolutional code compensates it (see Figure 3.5). Therefore, in the presence of the PHY mode 3, the PHY mode 2 may mot be a good choice for data delivery services. Another observation from Figure 3.7 is that a smaller MSDU size results in lower effective goodput due to the fixed amount of MAC/PHY layer overheads for each transmission attempt. Figure 3.8 shows the maximum effective goodput and the corresponding PHY mode selections for different SNR values. Notice that the PHY mode 2 is not part of the selections, which is consistent with the fact that the PHY mode 2 results in a smaller effective goodput than PHY mode 3 under all SNR conditions, as shown in Figure 3.7. In Figure 3.8, we can clearly observe the operating range for each PHY mode. Using these observations in Figure 3.5, the BERs for each PHY mode in their own operating range are quite small ($<10^{-4}$) compared to the collision probability ($>10^{-1}$, see Figure 3.3), which confirms the assumption in Section 3.1 that we ignore the effect of bit errors introduced by channel noise to derive the collision probability. This also implies that the operating range for each PHY mode ensures the link reliability with lower BER (or packet error rate).

Furthermore, we can use the same analytical method on the basic access method and derive the similar result, Figure 3.9, as Figure 3.8. Comparing these two figures, we observe that in the low SNR range, the RTS/CTS access method outperforms the basic access method with 2,000-octet MSDU, but loses its advantage in the higher SNR range. That implies we should extend our link adaptation algorithm to select MAC mechanisms as well. Table 3.1 and 3.2, derived from the comparison of some

numerical results with different MSDU size, MAC mechanisms and contending stations, list the selected PHY mode with the proper MAC mechanism corresponding to the given SNR range. From these two tables, an evident conclusion can be made. The longer the data payload is transmitted, the more likely the RTS/CTS access method is used. It happens to agree completely with the idea of using RTS_Threshold. But another observation makes the RTS_Threshold, the only parameter to decide whether the RTS/CTS access method is applied, insufficient. The observation is that even a 2,000-octet MSDU is transmitted (the upper limit of payload size is 2304 octets). The use of the basic access method is preferable in the high SNR range with the higher PHY mode. On the other hand, a 200-octet MSDU may be transmitted in the low SNR range will use the RTS/CTS access method with lower PHY mode. The rational behind this is that, the transmission duration of the data frame is the key factor not the length. Comparing Table 3.2 with 3.1, the more contending stations in the network, the more likely the RTS/CTS access method is chose because of the more potential collision events. Figure 3.10 shows the effect of the number of contending stations. The effective goodputs with different PHY modes decrease as the contending stations increase.

Figure 3.11 shows the system architecture for adopting LA algorithm. The link adaptor provides three levels of functionality. First, the link adaptor estimates the current SNR condition and the number of contending stations by monitoring the channel via the routing broadcast frames and previous transmission results. Second, the link adaptor selects the optimal combination of the PHY mode and MAC mechanism based on the SNR estimation, length of the data frame to be transmitted, and number of contending stations (see Table 3.1 and 3.2). The three functionalities are represented in the figure as the channel information estimator, MAC mechanism selector, and PHY mode selector, respectively.

Notice that this architecture is transparent to higher layers and can typically be implemented in existing networks. This makes it compatible with existing networks or higher layer applications. Besides, the basic idea of LA is to take advantage of the different modulation schemes, and FEC capabilities provided by IEEE 802.11a PHY and different MAC mechanisms provided by IEEE 802.11 MAC. Therefore, the implementation of the link adaptor should be fairly simple, which makes this algorithm more appealing.

3.6 Computer Simulations

In this section, we evaluate the effectiveness of the proposed LA algorithm using the NS-2 network simulator from LBNL [27]. We present modifications to this simulation environment to support 802.11a. We have modified NS-2 PHY and MAC layer parameters from 802.11b to 802.11a standard specification. These parameters include MAC and PHY header formats, data rates, and SIFS, DIFS, and EIFS time spacing as listed in Table 2.2. For the calculation of BER, the modulation curves shown in Figure 3.5 were implemented in the simulation model. The signal reception model looks up BER for a given SNR and uses this probability to determine whether the received frame with or without errors.

After constructing 802.11a model in NS-2, to verify the proposed algorithm, we simplify the simulation environment as a 2-node topology. The testing schemes under consideration are: six single-mode schemes using the PHY mode 1 (SM-1), mode 5 (SM-5) and mode 8 (SM-8) for both the basic and RTS/CTS access methods, respectively, and the proposed link adaptation scheme (LA). For each of the testing schemes, an experiment is repeated 10 times to estimate the average goodput for each

SNR value. At each experiment, the receiver requests a data delivery service of 10,000 MSDUs from the transmitter and the length of each MSDU is 2,000 octets using constant bit rate traffic generator.

Figure 3.12 shows the average goodputs obtained with SM-1, SM-5, SM-8, and LA. We can see that the simulation result confirms the theoretical analysis. The proposed algorithm switches to the higher PHY mode with increasing SNR and choose the proper access method to achieve the best goodput among other single mode schemes.

3.7 Summary

In this chapter, the goodput performance is derived analytically for peer-to-peer communication with numbers of contending stations in the IEEE 802.11a DCF system. The effective goodput is expressed as a closed-form function of the data payload length, wireless channel condition, number of contending stations in the same network, and selected transmission rate for both the basic and RTS/CTS access methods. Assuming the availability of the wireless channel conditions and number of contending stations, we propose an integrated LA algorithm, which selects the best combination of the PHY mode and MAC mechanism based on the theoretical analysis. We compare the performance of the proposed algorithm against three single-mode schemes by network simulator (NS-2). Simulation results show that the proposed algorithm works as expected.

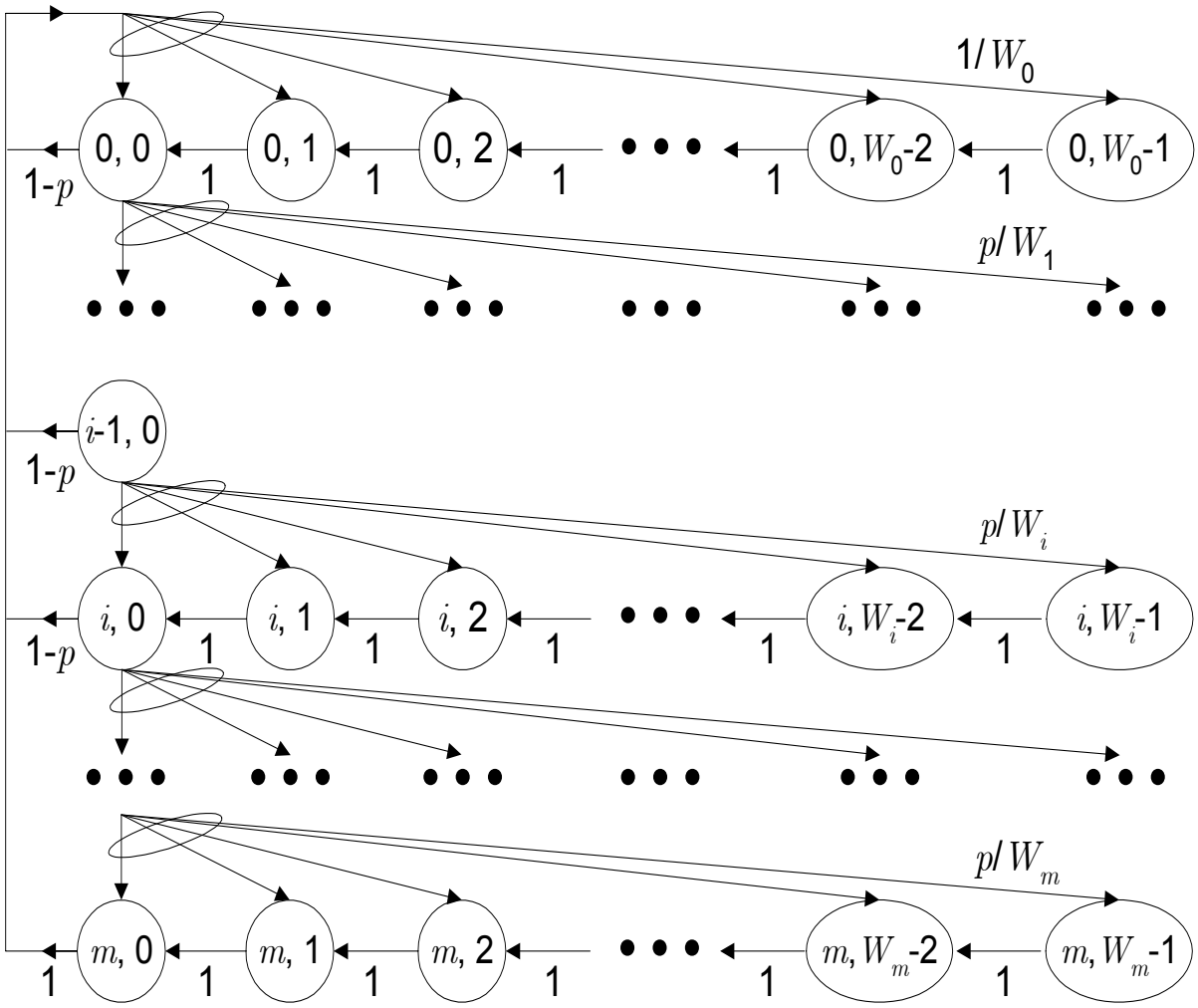

Figure 3.1: Markov chain model for the backoff window size

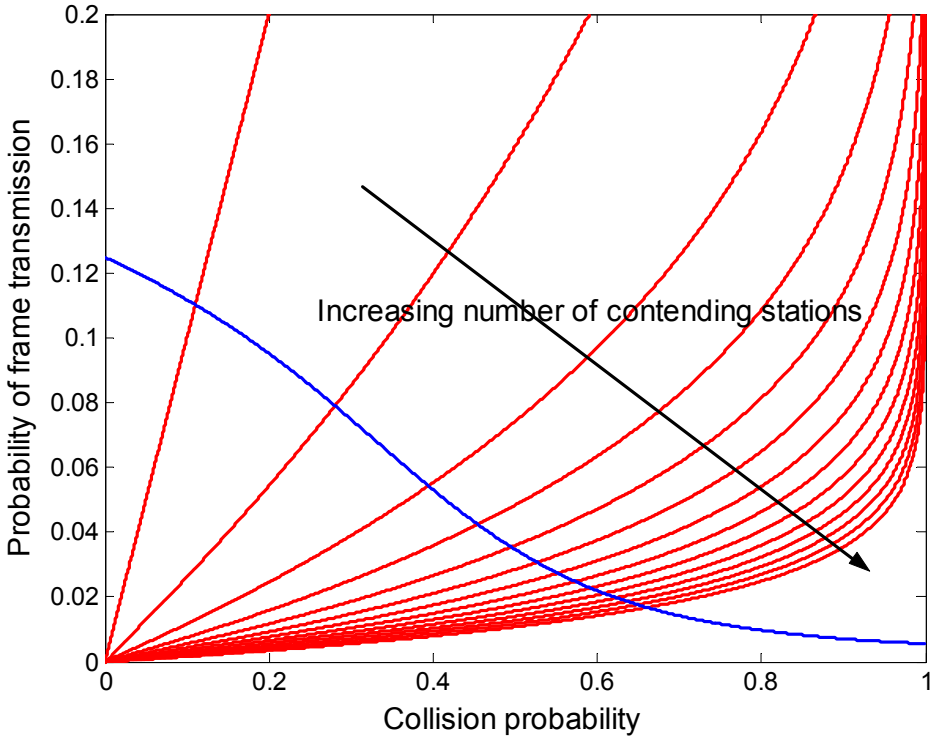

Figure 3.2: Solving for collision probability of IEEE 802.11a DCF system as the number of contending stations increases

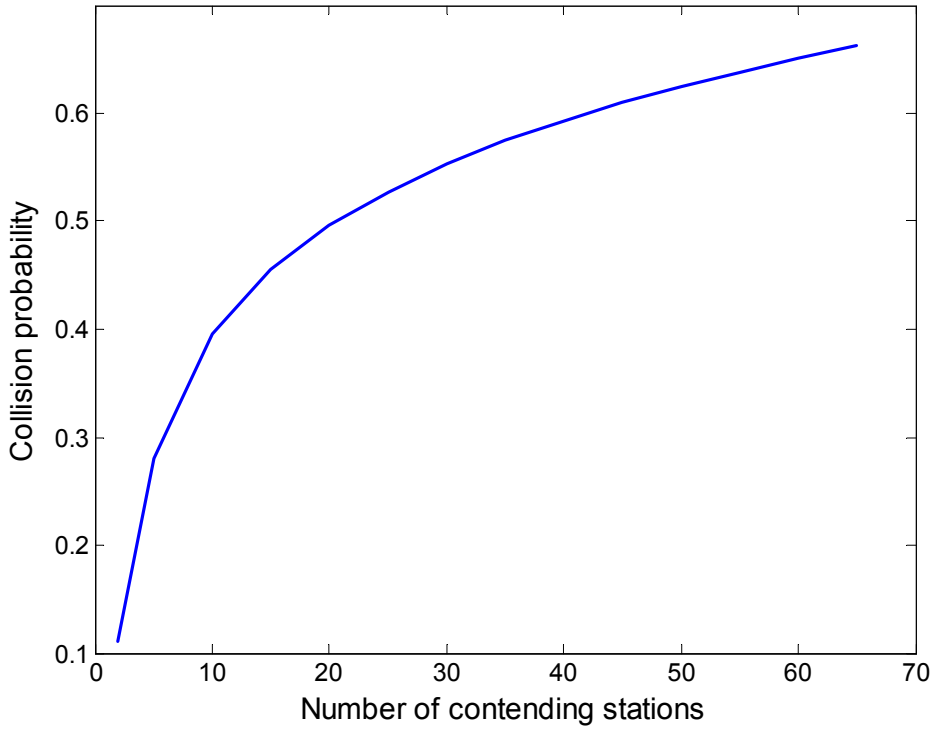

Figure 3.3: Collision probability of IEEE 802.11a DCF system versus the number of contending stations

(a)

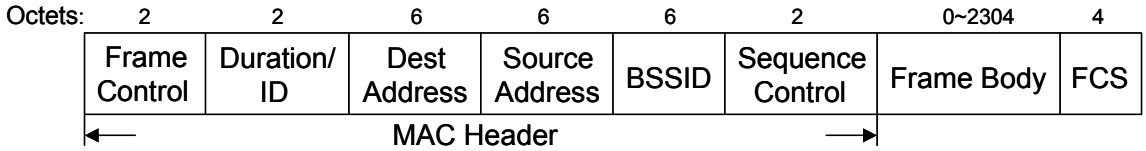

(b)

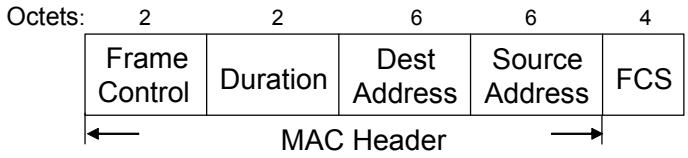

(c)

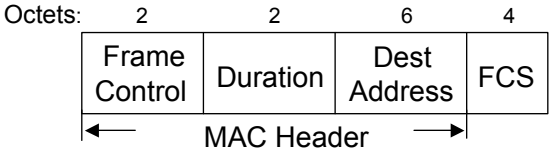

(d)

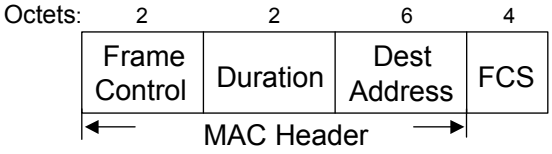

Figure 3.4: Frame formats of IEEE 802.11 MAC (a) Data frame (MPDU) (b) RTS frame (c) CTS frame (d) ACK frame

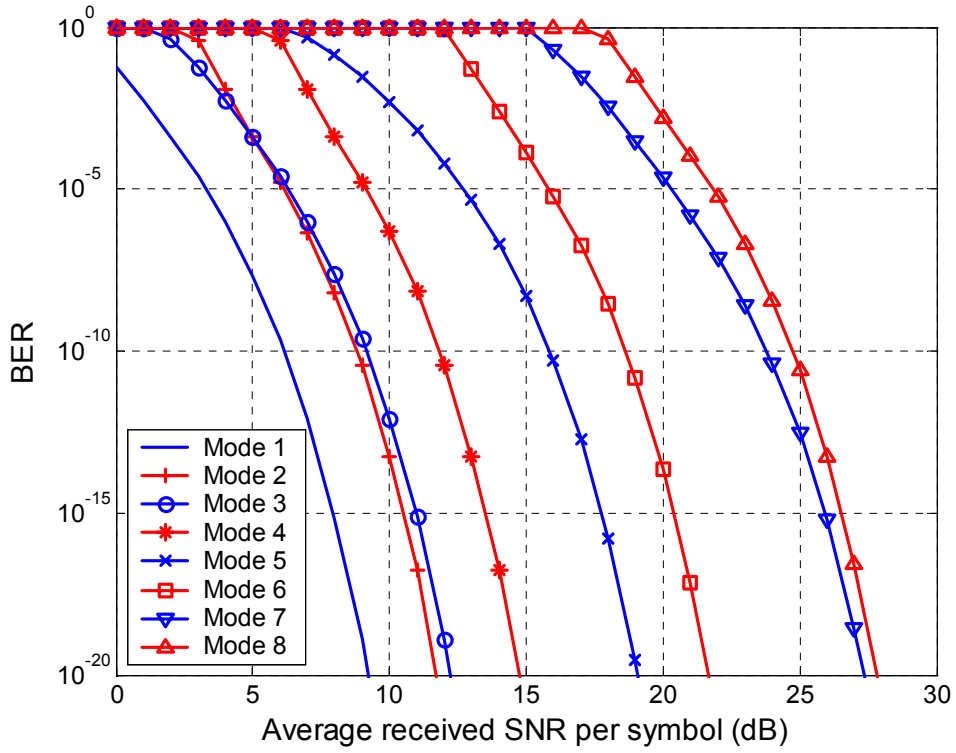

Figure 3.5: The upper bound BER performance of eight PHY modes of IEEE 802.11a versus the average received SNR per symbol

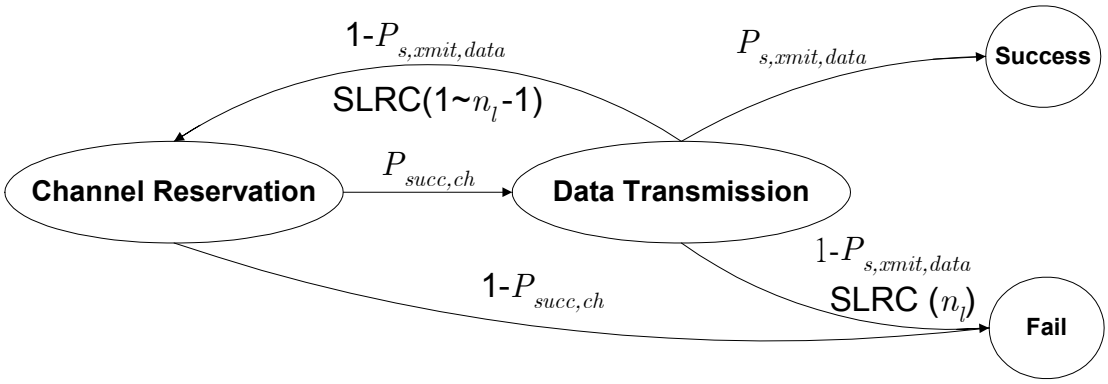

Figure 3.6: Two stages of RTS/CTS access method

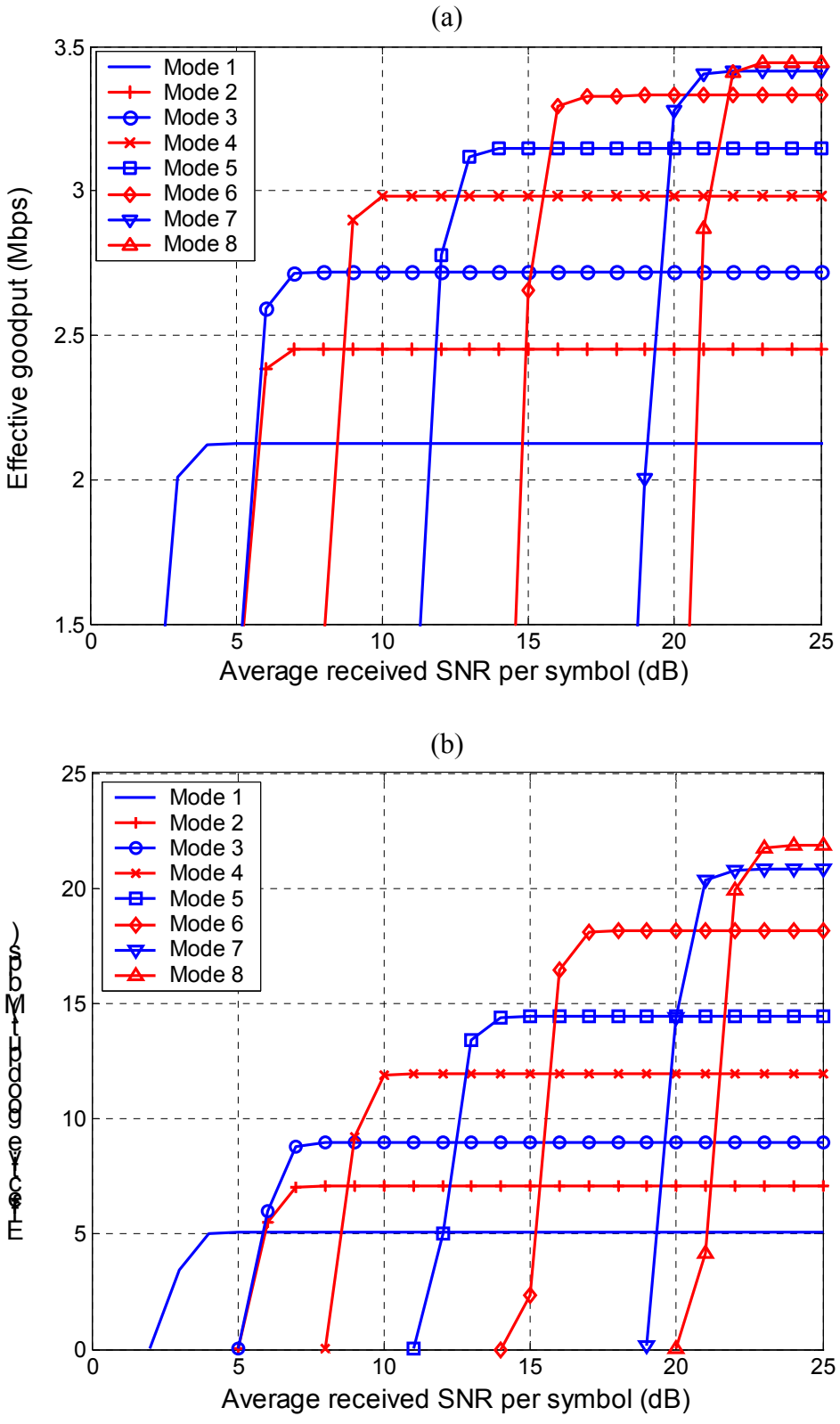

Figure 3.7: Effective goodputs of different PHY modes using RTS/CTS access method versus average received SNR per symbol. Assume there are five contending stations in IEEE 802.11a WLAN. (a) MSDU size: 200 octets (b) MSDU size: 2,000 octets

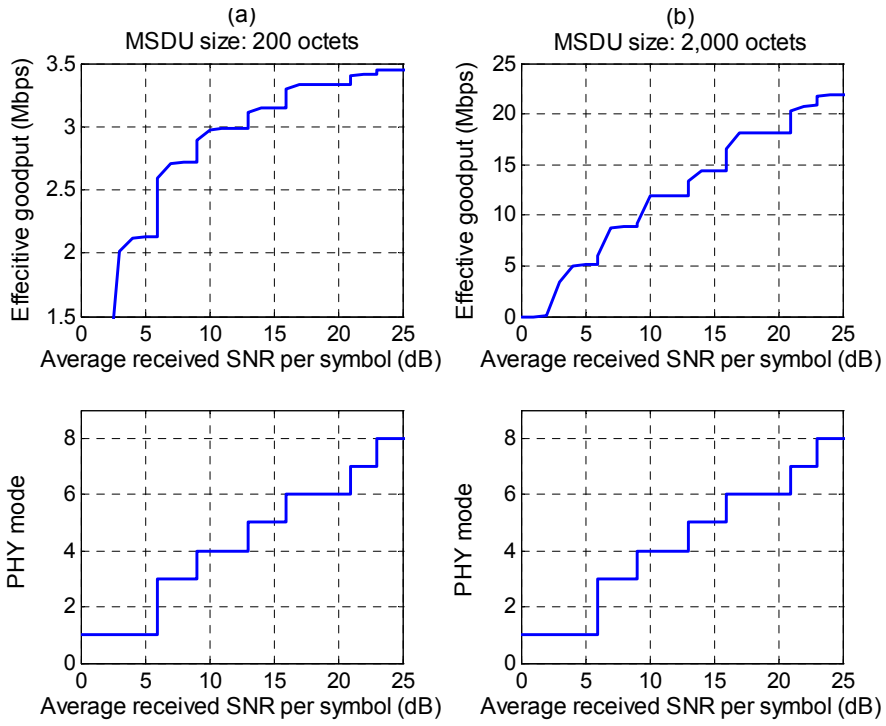

Figure 3.8: Adaptive PHY mode selection for improving the effective goodput using RTS/CTS access method in IEEE 802.11a WLAN with five contending stations. (a) MSDU size: 200 octets (b) MSDU size: 2,000 octets

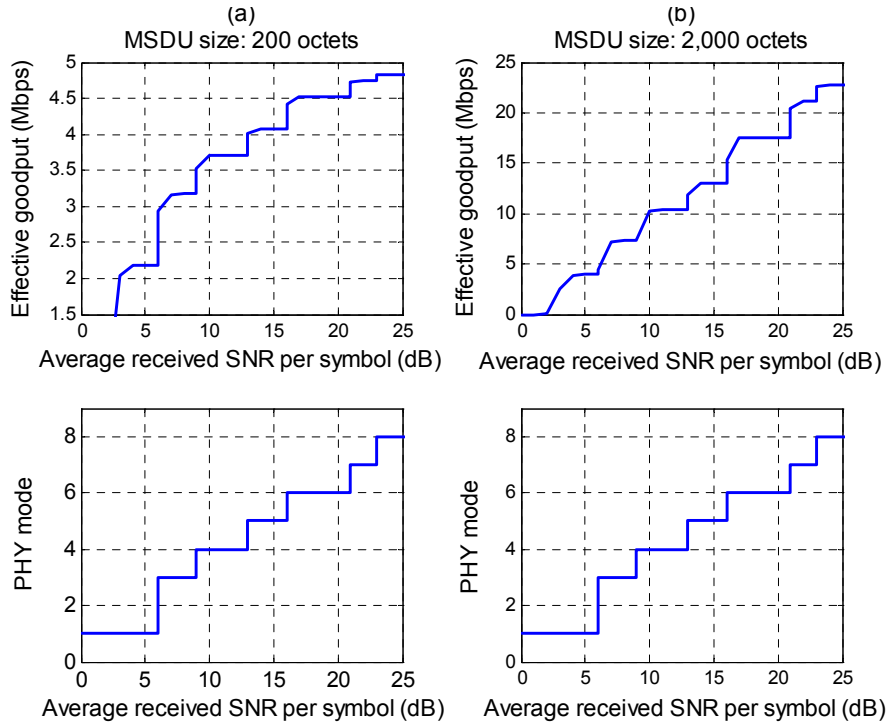

Figure 3.9: Adaptive PHY mode selection for improving the effective goodput using basic access method in IEEE 802.11a WLAN with five contending stations. (a) MSDU size: 200 octets (b) MSDU size: 2,000 octets

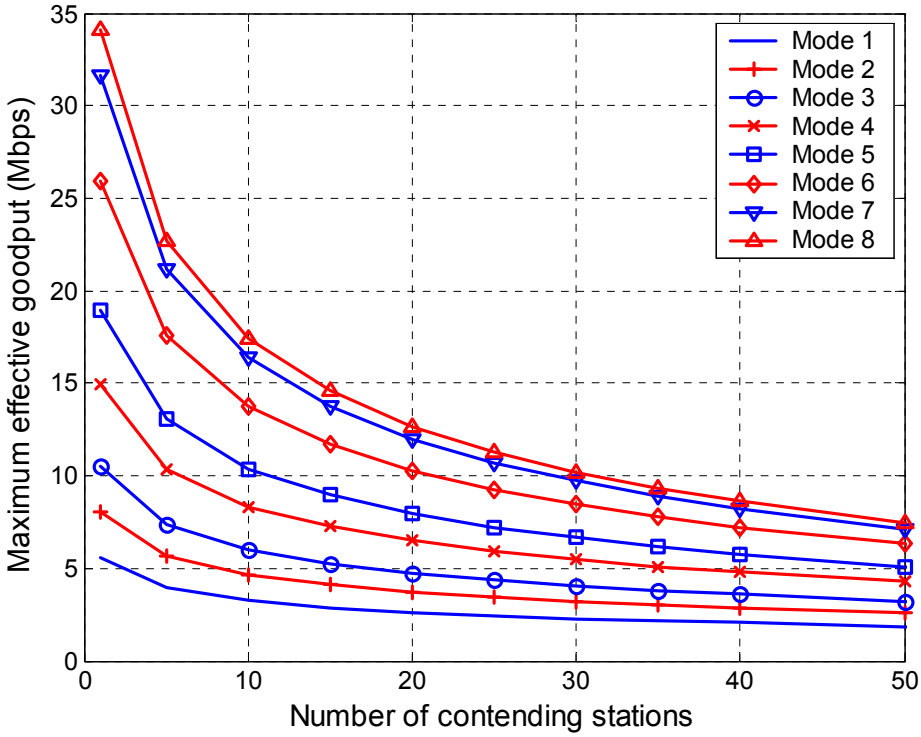

Figure 3.10: Maximum effective goodput of different PHY modes using basic access method versus number of contending stations in IEEE 802.11a WLAN. MSDU size: 2,000 octets.

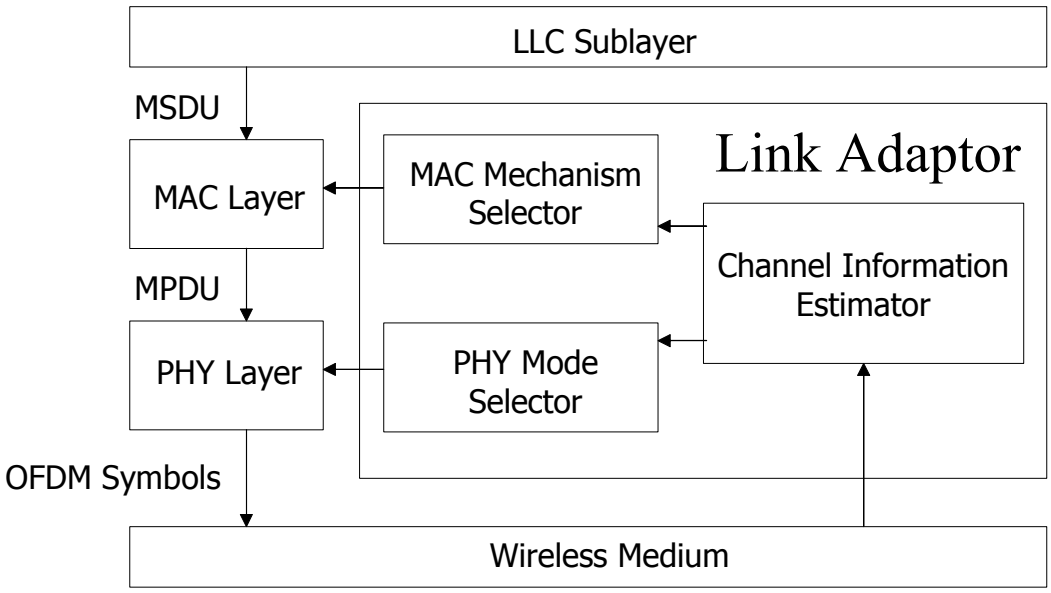

Figure 3.11: Proposed system architecture for link adaptation

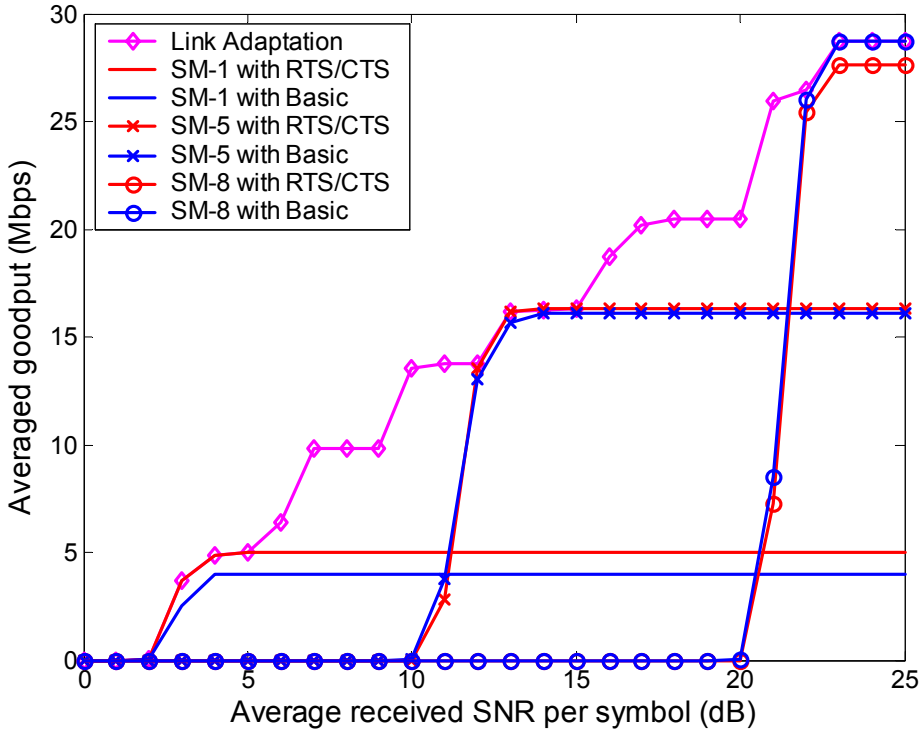

Figure 3.12: Performance evaluation for proposed link adaptation by NS-2 with 2-node topology. 2,000-octet MSDU is generated with CBR traffic.

Table 3.1: Adaptive PHY mode and MAC mechanism selection corresponding to given channel condition with five contending stations. Deep color represents RTS/CTS access method while light one stands for basic access method. (a) MSDU size: 200 octets (b) MSDU size: 500 octets (c) MSDU size: 1,000 octets (d) MSDU size: 2,000 octets

(a)

	Mode 1	Mode 3	Mode 4	Mode 5	Mode 6	Mode 7	Mode 8
SNR (dB)	~6	6~9	9~13	13~16	16~21	21~23	23~

(b)

	Mode 1	Mode 3	Mode 3	Mode 4	Mode 5	Mode 6	Mode 7	Mode 8
SNR (dB)	~6	6~7	7~9	9~13	13~16	16~21	21~23	23~

(c)

	Mode 1	Mode 3	Mode 4	Mode 5	Mode 5	Mode 6	Mode 7	Mode 8
SNR (dB)	~6	6~9	9~13	13~14	14~16	16~21	21~23	23~

(d)

	Mode 1	Mode 3	Mode 4	Mode 5	Mode 6	Mode 7	Mode 8
SNR (dB)	~6	6~9	9~13	13~16	16~21	21~23	23~

Table 3.2: Adaptive PHY mode and MAC mechanism selection corresponding to given channel condition with 20 contending stations. Deep color represents RTS/CTS access method while light one stands for basic access method. (a) MSDU size: 200 octets (b) MSDU size: 500 octets (c) MSDU size: 1,000 octets (d) MSDU size: 2,000 octets

(a)

	Mode 1	Mode 3	Mode 3	Mode 4	Mode 5	Mode 6	Mode 7	Mode 8
SNR (dB)	~6	6~7	7~9	9~13	13~16	16~21	21~23	23~

(b)

	Mode 1	Mode 3	Mode 4	Mode 5	Mode 6	Mode 7	Mode 8
SNR (dB)	~6	6~9	9~13	13~16	16~21	21~23	23~

(c)

	Mode 1	Mode 3	Mode 4	Mode 5	Mode 6	Mode 7	Mode 7	Mode 8
SNR (dB)	~6	6~9	9~13	13~16	16~21	21~22	22~23	23~

(d)

	Mode 1	Mode 3	Mode 4	Mode 5	Mode 6	Mode 7	Mode 8
SNR (dB)	~6	6~9	9~13	13~16	16~21	21~23	23~

Chapter 4

Link Adaptation for MIMO-Enhanced 802.11a Systems

The main goal in developing next generation wireless communication systems is to increase the link throughput. Significant improvements in throughput can be achieved when multiple antennas are applied at both the transmitter and receiver side, i.e. multiple-input multiple-output (MIMO) systems, especially in a rich scattering environment. This has been shown for wireless communication links in both flat-fading [12] as well as frequency-selective channels [16]. A potential application of the MIMO systems is next generation WLANs. An advantage of WLAN systems is that they are mainly deployed in indoor environments. These environments are typically characterized by richly scattered multipaths. As explained in [12], this is a good condition for having a high MIMO capacity.

In a MIMO system, the benefit of transmitting from multiple antennas may be utilized to improve either the diversity order or information rate of the system. These two transmission strategies are commonly denoted as spatial diversity and spatial multiplexing, respectively. Therefore, MIMO coding techniques can basically be split into two groups:

- Spatial diversity [13], e.g. space-time block code (STBC) [14][15], increases

the performance of the communication system by coding over the different transmit branches.

- Spatial multiplexing [12][16][17], e.g. Bell laboratories layered space-time (BLAST) [19], achieves a higher throughput by transmitting independent data streams on the different transmit branches simultaneously and at the same carrier frequency.

While STBC improves the link quality of the system by exploiting the spatial and temporal diversity, BLAST significantly improves the spectral efficiency of the system while suffering from poor error performance. In this chapter, we aim to compare these two techniques using the performance metric of effective goodput defined in Chapter 3 and select the most suitable MIMO technique under the given channel condition to increase the link throughput in an OFDM-based WLAN system with MIMO coding, while focusing on the IEEE 802.11a standard.

This chapter is organized as follows: Section 4.1 introduces the system models and performance analyses of STBC and VBLAST. According to the analysis results, we have to adopt the RTS/CTS exchange to obtain the MIMO channel information in the proposed LA algorithm in Section 4.2. For the purpose of carrying adaptive selection information based on the proposed LA algorithm, we modify the IEEE 802.11a MAC/PHY layer overheads in Section 4.3. Finally, we evaluate the proposed LA algorithm in Section 4.4.

4.1 MIMO Systems

4.1.1 MIMO Channel Model

The most commonly used channel model for MIMO systems involves independent quasi-static flat Rayleigh fading at all antenna elements [15][28][29]. The basic assumptions behind this channel model are:

1. A large number of scatters are present in the wireless channel so that the signal at any receive antenna of the MIMO systems is the sum of several multipath components. In this case, the distribution of the received signal at each antenna will be complex Gaussian. The amplitude of such complex Gaussian distributed signals is Rayleigh distributed.
2. The channel delay spread is less than the symbol rate (i.e. narrowband transmission). This assumption guarantees flat fading.
3. The channel characteristics remain constant at least for the transmission period of an entire frame. This assumption accounts for quasi-static fading.
4. The antenna elements at the transmitter and receiver of the MIMO system are placed far enough (spatially) such that the effect of the channel at a particular antenna element is different from the effect at all other antenna elements. This supports the assumption of independent or spatially uncorrelated fading.

Using all these assumptions, the independent quasi-static flat Rayleigh fading MIMO channel for a system with n_T transmit and n_R receive antennas can be represented as

$$\mathbf{H} = \begin{bmatrix} h_{1,1} & h_{1,2} & \cdots & h_{1,n_T} \\ h_{2,1} & h_{2,2} & \cdots & h_{2,n_T} \\ \vdots & \vdots & \ddots & \vdots \\ h_{n_R,1} & h_{n_R,2} & \cdots & h_{n_R,n_T} \end{bmatrix} \tag{4.1}$$

where $h_{i,j}$ is the path gain. This is the effect of the channel on signals transmitted from jth transmit antenna and received at the ith receive antenna. The path gains are modeled as zero mean independent complex Gaussian random variables with variance 0.5 per real dimension. Therefore, given that the signal x_j is transmitted from the jth transmit antenna, the signal received at the ith receive antenna is given by

$$y_i = \sum_{j=1}^{n_T} h_{i,j} \cdot x_j + n_i \ , \quad i = 1,2,\cdots,n_R \tag{4.2}$$

The additive noise n_i at each receive antenna i is assumed to be white and Gaussian with spectral density N_0.

However, broadband wireless systems encounter a large delay spread, and therefore have to cope with frequency-selective fading. In this chapter, we focus on OFDM-based WLAN systems with MIMO coding, i.e. MIMO-OFDM systems. A K-subcarrier MIMO-OFDM system divides the large bandwidth into K narrow subbands, hence it decouples the frequency-selective MIMO channel into a set of K parallel MIMO channels [30]. Thus, in each subband, the model given above can be used.

4.1.2 Performance Analysis of STBC-Enhanced 802.11a PHY

A simple case of STBC proposed by Alamouti consists of two antennas at the transmitter and any number of receive antennas [14]. The case of two antennas at both the transmitter and receiver is considered in this chapter. For a given subband k, the Alamouti's scheme for two transmit antennas is determined by the complex orthogonal design

$$\mathbf{B} = \begin{bmatrix} x_1^k & x_2^k \\ -x_2^{k*} & x_1^{k*} \end{bmatrix} \tag{4.3}$$

where x_1^k and x_2^k are transmitted from antennas 1 and 2 respectively at a given time t. In the following OFDM symbol at time $t+T$, $-x_2^{k^*}$ is transmitted from antenna 1 while antenna 2 transmits $x_1^{k^*}$, where $x_1^{k^*}$ and $x_2^{k^*}$ represent the complex conjugates of x_1^k and x_2^k. The mean energy per symbol is given by

$$E\left\{x_i^k x_i^{k^*}\right\} = \frac{E_s}{n_T} = \frac{E_s}{2} \tag{4.4}$$

The kth-subband channels between the transmit and receive antennas can be expressed as follows:

$$\mathbf{H}_t^k = \mathbf{H}_{t+T}^k = \begin{bmatrix} h_{1,1}^k & h_{1,2}^k \\ h_{2,1}^k & h_{2,2}^k \end{bmatrix} \tag{4.5}$$

The signal arriving at the receive antenna is a noisy superposition of the faded version of the transmitted OFDM symbols. After passing through the FFT process, the following received signals can be generated:

At time t:

$$\begin{aligned} y_{1,t}^{k} &= x_1^k h_{1,1}^k + x_2^k h_{1,2}^k + n_{1,t}^k \\ y_{2,t}^{k} &= x_1^k h_{2,1}^k + x_2^k h_{2,2}^k + n_{2,t}^k \end{aligned} \tag{4.6}$$

At time t+T:

$$\begin{aligned} y_{1,t+T}^{k} &= -x_2^{k^*} h_{1,1}^k + x_1^{k^*} h_{1,2}^k + n_{1,t+T}^k \\ y_{2,t+T}^{k} &= -x_2^{k^*} h_{2,1}^k + x_1^{k^*} h_{2,2}^k + n_{2,t+T}^k \end{aligned} \tag{4.7}$$

where $n_{1,t}$, $n_{2,t}$, $n_{1,t+T}$, and $n_{2,t+T}$ represent uncorrelated complex random AWGN. We can rewrite (4.6), (4.7) as

$$\widetilde{\mathbf{Y}}_k = \begin{bmatrix} y_{1,t}^k \\ y_{2,t}^k \\ y_{1,t+T}^{k\ *} \\ y_{2,t+T}^{k\ *} \end{bmatrix} = \begin{bmatrix} h_{1,1}^k & h_{1,2}^k \\ h_{2,1}^k & h_{2,2}^k \\ h_{1,2}^{k\ *} & -h_{1,1}^{k\ *} \\ h_{2,2}^{k\ *} & -h_{2,1}^{k\ *} \end{bmatrix} \begin{bmatrix} x_1^k \\ x_2^k \end{bmatrix} + \begin{bmatrix} n_{1,t}^k \\ n_{2,t}^k \\ n_{1,t+T}^{k\ *} \\ n_{2,t+T}^{k\ *} \end{bmatrix} = \widetilde{\mathbf{H}}_k \mathbf{X}_k + \tilde{\mathbf{n}}_k \tag{4.8}$$

Left-multiplying (4.8) by the transposed and conjugate channel matrix $\widetilde{\mathbf{H}}_k^{\mathbf{H}}$, i.e.

$$\begin{aligned} \widehat{\mathbf{Y}}_k &= \widetilde{\mathbf{H}}_k^{\mathbf{H}} \widetilde{\mathbf{H}}_k \mathbf{X}_k + \widetilde{\mathbf{H}}_k^{\mathbf{H}} \tilde{\mathbf{n}}_k \\ &= \widetilde{\mathbf{H}}_k^{\mathbf{H}} \widetilde{\mathbf{H}}_k \mathbf{X}_k + \hat{\mathbf{n}}_k \end{aligned} \tag{4.9}$$

using

$$\widetilde{\mathbf{H}}_k^{\mathbf{H}} \widetilde{\mathbf{H}}_k = \begin{bmatrix} \left|h_{1,1}^k\right|^2 + \left|h_{2,1}^k\right|^2 + \left|h_{1,2}^k\right|^2 + \left|h_{2,2}^k\right|^2 & 0 \\ 0 & \left|h_{1,1}^k\right|^2 + \left|h_{2,1}^k\right|^2 + \left|h_{1,2}^k\right|^2 + \left|h_{2,2}^k\right|^2 \end{bmatrix} \tag{4.10}$$

yields

$$\begin{aligned} \hat{y}_1^k &= \left(\left|h_{1,1}^k\right|^2 + \left|h_{2,1}^k\right|^2 + \left|h_{1,2}^k\right|^2 + \left|h_{2,2}^k\right|^2\right) x_1^k + \hat{n}_1^k \\ \hat{y}_2^k &= \left(\left|h_{1,1}^k\right|^2 + \left|h_{2,1}^k\right|^2 + \left|h_{1,2}^k\right|^2 + \left|h_{2,2}^k\right|^2\right) x_2^k + \hat{n}_2^k \end{aligned} \tag{4.11}$$

where

$$\begin{aligned}\hat{n}_1^k &= {h_{1,1}^k}^* n_{1,t}^k + {h_{2,1}^k}^* n_{2,t}^k + h_{1,2}^k {n_{1,t+T}^k}^* + h_{2,2}^k {n_{2,t+T}^k}^* \\ \hat{n}_2^k &= {h_{1,2}^k}^* n_{1,t}^k + {h_{2,2}^k}^* n_{2,t}^k - h_{1,1}^k {n_{1,t+T}^k}^* - h_{2,1}^k {n_{2,t+T}^k}^*\end{aligned} \tag{4.12}$$

The variance per real dimension of the additive white Gaussian noise $\hat{n}_i^k$ is given by

$$\sigma_{\hat{n}}^2 = \sigma^2 \cdot \sum_{i=1}^{2} \sum_{j=1}^{2} \left| h_{i,j}^k \right|^2 \tag{4.13}$$

where σ^2 is the variance per real dimension of the noise at each of the receive antennas, i.e. $\sigma^2 = \frac{N_0}{2}$.

Thus, due to the orthogonal structure of STBC, we obtain decoupled equations for x_1^k and x_2^k. The equation (4.11) corresponds to the maximum ration combining. Figure 4.1 and 4.2 illustrates the linear combining and the resulting equivalent maximum ratio combining model. Furthermore, We can see that STBC together with a linear combiner at the receiver transform the fading MIMO channel towards an SISO channel with a lower probability of deep fades compared to the channel from a certain transmit antenna to a certain receive antenna. Consequently, STBC, the fading MIMO channel, and linear combiner can be described by an equivalent scaled AWGN channel model as depicted in Figure 4.3, which is determined by

$$\hat{y}_i^k = \left\| \mathbf{H}_k \right\|_F^2 x_i^k + \hat{n}_i^k \tag{4.14}$$

The resulting channel gain is given by

$$\left\| \mathbf{H}_k \right\|_F^2 = \sum_{i=1}^{n_R} \sum_{j=1}^{n_T} \left| h_{i,j}^k \right|^2 = \sum_{i=1}^{2} \sum_{j=1}^{2} \left| h_{i,j}^k \right|^2 \tag{4.15}$$

which is the squared Frobenius norm of $\mathbf{H}_k$. Therefore, the effective instantaneous received SNR in subband k at the receiver is

$$\gamma_k = \frac{E_s}{n_T \cdot N_0} \left\| \mathbf{H}_k \right\|_F^2 = \frac{E_s}{2N_0} \left\| \mathbf{H}_k \right\|_F^2 \tag{4.16}$$

From this result, we can obtain the instantaneous error performances of different PHY modes with the STBC-enhanced 802.11a system using the formulas in Section 3.3. The results are depicted in Figure 4.4 with the flat Rayleigh fading channel matrix $\mathbf{H} = \begin{bmatrix} 0.0079513 - 0.69987i & 0.56974 + 0.20471i \\ -0.45619 + 0.94723i & 0.16378 + 1.0458i \end{bmatrix}$. Compared with Figure 3.5, we can see that the effect of STBC provides an SNR gain in the STBC-enhanced 802.11a system. It clearly improves the error performance of each PHY mode, i.e. making the data transmission more reliable.

4.1.3 Performance Analysis of VBLAST-Enhanced 802.11a PHY

The main idea of the BLAST architecture is to split the information bit stream into several sub-streams of equal length (called layers) and transmit them in parallel using a set of transmit antennas (the number of transmit antennas equals the number of sub-streams) at the same time and frequency. VBLAST (vertical BLAST) is known as a simplified version of the BLAST algorithm [31]. It is capable of achieving high spectral efficiency while being relatively simple to implement [32]. The layers are vertically arranged and each of them is transmitted over one particular antenna as shown in Figure 4.5. We use the same MIMO-OFDM system as in Section 4.1.2. The received signal vector in subband *k* can be written as

$$\mathbf{Y}_k = \begin{bmatrix} y_1^k \\ y_2^k \end{bmatrix} = \begin{bmatrix} h_{1,1}^k & h_{1,2}^k \\ h_{2,1}^k & h_{2,2}^k \end{bmatrix} \cdot \begin{bmatrix} x_1^k \\ x_2^k \end{bmatrix} + \begin{bmatrix} n_1^k \\ n_2^k \end{bmatrix} = \mathbf{H}_k \mathbf{X}_k + \mathbf{n}_k \tag{4.17}$$

where $\mathbf{X}_k = \sqrt{\frac{E_s}{n_T}}\mathbf{S}_k = \sqrt{\frac{E_s}{2}}\mathbf{S}_k$ and $E\left\{s_i^k s_i^{k^*}\right\} = 1$. The received signal is a

superposition of all transmitted symbols scaled by the channel gain and corrupted by AWGN. Assume the receiver uses a ML detection criterion based on perfect channel knowledge. The estimated symbol vector in the subband k is

$$\hat{\mathbf{S}}_k = \arg\min_{\mathbf{S}_k} \left\| \mathbf{Y}_k - \sqrt{\frac{E_s}{2}} \mathbf{H}_k \mathbf{S}_k \right\|_F^2 \tag{4.18}$$

where the minimization is performed over all admissible vectors $\mathbf{S}_k$. An error occurs when the receiver mistakes a transmitted vector for another vector from the set of possible vectors. The probability that the receiver mistakes the transmitted vector $\mathbf{S}_k^i$ for another vector $\mathbf{S}_k^j$, given knowledge of the channel realization at the receiver (also referred to as the pairwise error probability), is [33][34]

$$\begin{aligned} P\left(\mathbf{S}_k^i \to \mathbf{S}_k^j \mid \mathbf{H}_k\right) &= Q\left(\sqrt{\frac{E_s \left\| \mathbf{H}_k \left(\mathbf{S}_k^i - \mathbf{S}_k^j\right) \right\|_F^2}{2 n_T N_0}}\right) \\ &\le Q\left(\sqrt{\frac{\gamma}{4} D_{k,\min}^2}\right) \end{aligned} \tag{4.19}$$

where $D_{k,\min}^2 = \min_{i,j} \left\| \mathbf{H}_k \left(\mathbf{S}_k^i - \mathbf{S}_k^j\right) \right\|_F^2$ is the squared minimum distance of the separation of the vector constellation points at the receiver. Using the Rayleigh-Rits criterion, we can bound $D_{k,\min}^2$ by

$$D_{k,\min}^2 \ge \lambda_{k,\min}^2 d_{k,\min}^2 \tag{4.20}$$

where $\lambda_{k,\min}^2$ is the squared minimum singular value of $\mathbf{H}_k$, and $d_{k,\min}^2$ is the squared minimum distance of the transmit scalar constellation. Therefore, we can get the upper bound of the instantaneous SER for VBLAST transmission

$$P_{s,VBLAST} \le Q\left(\sqrt{\frac{\gamma}{4} \lambda_{k,\min}^2 d_{k,\min}^2}\right) \tag{4.21}$$

With a Gray coding, BER can be approximated by

$$P_{b,VBLAST} \approx \frac{1}{N} \cdot P_{s,VBLAST} \tag{4.22}$$

where N is the bit numbers modulated into one symbol. Figure 4.6 shows the performance of the QPSK modulated VBLAST system compared with the derived upper bound over the flat Rayleigh fading channel matrix $\mathbf{H} = \begin{bmatrix} 0.0079513 - 0.69987i & 0.56974 + 0.20471i \\ -0.45619 + 0.94723i & 0.16378 + 1.0458i \end{bmatrix}$. The result confirms the performance analysis in this section. From (4.22), we can obtain the instantaneous error performance of different PHY modes with the VBLAST-enhanced 802.11a system using the formulas in Section 3.3. Figure 4.7 illustrates the obtained results with the same channel matrix as before.

4.2 Link Adaptation Scheme

In (4.16), the instantaneous received SNR of the STBC-enhanced 802.11a system is governed by the squared Frobenius norm of the channel matrix $\mathbf{H}_k$, that is to say the squared Frobenius norm of channel matrix $\mathbf{H}_k$ determines the performance of the STBC-enhanced 802.11a system. On the other hand, (4.21) shows that a larger value of $\lambda_{k,\min}$ guarantees a smaller error probability of the VBLAST-enhanced 802.11a system. The performance of the VBLAST-enhanced 802.11a is strongly linked to the smallest singular value of the channel matrix $\mathbf{H}_k$. Therefore, the complete channel information is required to evaluate the performances for both the STBC and VBALST systems for selecting these two schemes. We adopt the RTS/CTS exchange to obtain the channel information and perform LA. The receiver estimates the channel

information while receiving the RTS frame, then it uses this information to computes the effective goodput defined in Chapter 3, the metric for selecting the appropriate transmission scheme, and feeds the decision back to the transmitter via the CTS frame.

For this purpose, we modified the algorithm proposed by [8]. In [8], instead of carrying the duration of the reservation, the frames carry the data rate and data frame length. We add into one more parameter, the MIMO scheme. This modification serves the dual purpose of providing a mechanism by which the receiver can communicate the chosen transmission strategy to the transmitter, while still providing neighboring nodes with enough information to calculate the duration of the requested reservation. The detailed algorithm is as follows.

At the first, the transmitter chooses the transmission strategy as the lowest rate PHY mode, i.e. STBC with the BPSK modulation and rate-1/2 convolutional coding, and then stores the corresponding parameters into the RTS frame. This ensures the reservation period is the most robust. The neighboring nodes hearing the RTS frame calculate the duration of the requested reservation, D_{rts}, using the information carried in the RTS frame and update its NAV. The receiver uses the RTS frame to estimate the channel information and selects the appropriate transmission strategy based on this estimation. Then, it transmits the CTS frame with the selected MIMO scheme, data rate, and data frame length back to the transmitter. The neighboring nodes hearing the CTS frame calculate the duration of the requested reservation, D_{cts}, using the information carried in the CTS frame and update its NAV to account for the difference between D_{rts} and D_{cts}. Finally, the transmitter responds to the receipt of the CTS by transmitting the data frame with the transmission strategy chosen by the receiver.

In the instance that the transmission strategies chosen by the transmitter and

receiver are different, the reservation duration, D_{rts}, calculated by the information carried in the RTS frame is no longer valid. Thus, we refer to D_{rts} as a tentative reservation. A tentative reservation serves only to inform neighboring nodes that a reservation has been requested but the duration of the final reservation may differ. The tentative reservation effectively serves as a placeholder, denying any later requests that would conflict with it, until either a new reservation is received (D_{cts}) or it is confirmed as the final reservation. Final reservations are confirmed by the presence of a special subheader, called the reservation subheader (RSH), in the MAC header of the data frame. RSH consists of a subset of the header fields that are already present in the IEEE 802.11 data frame, plus a check sequence that serves to protect the subheader. The fields in RSH consist of those needed to update the NAV, and essentially preserve the same fields present in an RTS frame. Furthermore, the fields (minus the check sequence) still retain the same functionality that they have in a standard IEEE 802.11 header. The functionality of RSH is as follows: when transmitter sends the data frame with the special MAC header containing RSH. The nodes out of the CTS transmission range can use the information carried in RSH to calculate the final reservation, D_{rsh}, to update the NAV to account for the difference between D_{rts} and D_{rsh}.

Note that, for the neighboring nodes to update their NAV correctly, they must know what contribution D_{rts} has made to their NAV. This can be done by maintaining a list of the end times of each tentative reservation, indexed according to the (*transmitter*, *receiver*) pair. Thus, when an update is required, a node can use the list to determine if the difference in the reservation will require a change in the NAV.

4.3 Modified MAC/PHY Layer Overheads

Figure 3.4 shows the standard IEEE 802.11 frame formats. The DURATION fields in the RTS and CTS frames contain the D_{rts} and D_{cts} respectively. As the algorithm described above, the modification of the standard IEEE 802.11 frame formats is shown in Figure 4.8. A description of each modification is given next.

1. A new MAC data frame is introduced, shown in Figure 4.8(a), in which the standard IEEE 802.11 data frame has been changed to include a 32-bit check sequence positioned immediately after the SOURCE ADDRESS field. The check sequence is used to protect RSH, which consists of the FRAME CONTRL, DURATION, DESTINATION ADDRESS, and SOURCE ADDRESS fields. Besides, we interchange the BSSID and SEQUENCE CONTROL fields, and include the SEQUENCE CONTROL field in RSH. The reason for this will be discussed in the following description.
2. The RTS and CTS control frames, shown in Figure 4.8(b) and (c), have been changed to encode a 1-bit MIMO subfield, 3-bit RATE subfield, and 12-bit LENGTH subfield, in place of the 16-bit DURATION field in the standard IEEE 802.11 frames. The contents of the MIMO and RATE subfields are listed in Table 4.1 and 4.2. The LENGTH subfield gives the size of the data frame in octets.
3. The PPDU format, shown in Figure 4.9, has to adopt the modification in MAC data frames. The functionality of RSH is the same as the RTS frame. Thus, it should be transmitted by the most robust transmission mode, i.e. the BPSK modulation and rate-1/2 convolutional coding. We can see that the SERVICE field and reservation subheader together adds up to eight OFDM

symbols, that's why we interchange the BSSID and SEQUENCE CONTROL fields and include the sequence control fields in RSH.

Recall that, the use of the RTS/CTS exchange is to estimate the channel matrix between the transmitter and receiver. To achieve this purpose, the RTS frame must be transmitted by MIMO techniques [35][36]. Therefore, we sent the RTS frame, CTS frame, ACK frame, and PLCP with RSH are sent by STBC to increase the transmission reliability.

According to the modification described above, to transmit a frame with an *l*-octet data payload over the STBC-enhanced 802.11a system using PHY mode m, the transmission duration is

$$\begin{aligned} T_{data}(l,m) &= T_{PREAMBLE} + T_{SIGNAL} + T_{SERVICE+RSH} + \left\lceil \frac{10+6/8+l}{BpS(m)} \right\rceil \cdot T_{SYM} \\ &= 20\mu s + 32\mu s + \left\lceil \frac{10.75+l}{BpS(m)} \right\rceil \cdot 4\mu s \end{aligned} \quad (4.23)$$

On the other hand, over the VBLAST-enhanced 802.11a system, the transmission duration with PHY mode m is

$$\begin{aligned} T_{data}(l,m) &= T_{PREAMBLE} + T_{SIGNAL} + T_{SERVICE+RSH} + \left\lceil \frac{10/n_T+6/8+l/n_T}{BpS(m)} \right\rceil \cdot T_{SYM} \\ &= 20\mu s + 32\mu s + \left\lceil \frac{5.75+l/2}{BpS(m)} \right\rceil \cdot 4\mu s \end{aligned} \quad (4.24)$$

Note that, the coded data is split into two sub-streams transmitted in parallel via two transmit antennas. Similarly, the transmission duration for an RTS frame, a CTS frame, and an ACK frame are the same as (3.13), (3.14), and (3.15) respectively because the MAC frame sizes are unchanged and STBC has no improvement in data rate.

Therefore, we can compute the effective goodput in MIMO systems, as in Section 3.4, with the modified transmission durations for different frames in this section and error performances of different transmission strategies in Section 4.1.2 and 4.1.3.

Using this result as the selection metric in Section 4.2, we complete the whole link adaptation algorithm. The following section shows the computer simulations.

4.4 Computer Simulations

At first, we try to find some relation between the squared Frobenius norm and minimum singular value, the main factor for determining the performances of STBC and VBLST, of the MIMO channel matrix. We obtain 20 realizations of independent flat Rayleigh fading 2x2 MIMO channel matrix, and find their squared Frobenius norm and minimum singular value respectively. The results given in Figure 4.10 show that these two parameters of the MIMO channel have no obvious correlation between each other. Therefore, the switching threshold between STBC and VBLAST may differ with every independent MIMO channel matrix (see Table 4.3 and 4.4). Considering nodes A and B in Figure 4.10, node A represents the channel matrix $\mathbf{H}_1 = \begin{bmatrix} 0.0079513\text{-}0.69987i & 0.56974+0.20471i \\ -0.45619+0.94723i & 0.16378+1.0458i \end{bmatrix}$ and node B represents the channel matrix $\mathbf{H}_2 = \begin{bmatrix} 0.26894+3.0541e\text{-}005i & -0.013796+0.77428i \\ -0.71355\text{-}0.22476i & -0.034097\text{-}1.3251i \end{bmatrix}$. They have almost the same squared Frobenius norm (about mean squared Frobenius norm, 4) but quite different minimum singular value. We take these two MIMO channel realizations to compute the effective goodput of STBC and VBLAST enhanced 802.11a systems with MSDU size of 2,000 octets and five contending stations, and the comparison results are listed in Table 4.3 and 4.4. As expected, the STBC is chosen in the low SNR range while VBLAST is preferred in the high SNR range for their underlying functionalities. The resulting maximum goodputs based on the adaptive PHY mode and MIMO coding

selection listed in Table 4.3 and 4.4 are depicted in Figure 4.11. Note that, since the squared Frobenius norms of both channel matrices are almost the same, the performances in the low SNR range are similar due to the same operating MIMO coding, STBC. But the difference between the minimum singular values results in a great performance gap in the high SNR range. The rationale behind this is that, the VBLAST which provides high spectral efficiency experiences fewer errors with the bigger minimum singular value. In other words, the MIMO system whose channel matrix has a larger minimum singular value utilizes the spectrum more efficiently.

Compared to the standard IEEE 802.11a system with the RTS/CTS access method discussed in Chapter 3, assuming that the instantaneous channel gain is equal to $E\left\{\left|h_{i,j}\right|^2\right\}=1$, the MIMO enhanced 802.11a systems indeed improve the goodput as shown in Figure 4.12. In the SNR range from 24 to 34 dB, the MIMO enhanced 802.11a system with channel matrix $\mathbf{H}_2$ loses its advantage due to the modified data frame format. In this range, it chooses the PHY mode 8 as does the standard IEEE 802.11a system. But the modified data frame format consists of eight OFDM symbols (including the SERVICE and RSH fields) transmitted with the lowest PHY mode, which is transmitted with the highest PHY mode in the standard IEEE 802.11a system in the mentioned SNR range. Therefore, it incurs additional transmission time for overheads, which degrades the resulting goodput. Fortunately, the influence is negligibly small.

Another observation is that VBLAST increases only about 20% maximum goodput of the IEEE 802.11a WLAN. It might conflict with the twice data rate VBLAST provides. However, the increased data rate is only beneficial for MPDU. Other PHY overheads and a part of MAC headers are transmitted with the original data rate. Using (4.23) and (4.24), we can show the transmission duration for both STBC

and VBLAST with 2,000 octets and PHY mode 8 in the best scenario, i.e. no errors occur during the progress of the transmission, as follows.

STBC :

$$\begin{aligned} &\overline{T}_{bkoff}(1) + T_{rts} + T_{cts} + T_{data} + T_{ack} + 3tSIFSTime + tDIFSTime \\ &\Rightarrow 67.5 + 52 + 44 + (20 + 32 + \left\lceil \frac{2010.75}{27} \right\rceil \times 4) + 24 + 3 \times 16 + 34 = 641.5\mu s \end{aligned} \tag{4.25}$$

VBLAST :

$$\Rightarrow 67.5 + 52 + 44 + (20 + 32 + \left\lceil \frac{1005.75}{27} \right\rceil \times 4) + 24 + 3 \times 16 + 34 = 493.5\mu s$$

The corresponding goodput is

STBC :

$$\frac{2000 \times 8}{641.5 \times 10^{-6}} = 24.94 \text{ (Mbps)}$$

VBLAST : (4.26)

$$\frac{2000 \times 8}{493.5 \times 10^{-6}} = 32.42 \text{ (Mbps)}$$

Therefore, we know that VBLAST can only increase about 30% goodput compared to STBC at best due to the unavoidable MAC/PHY overheads.

4.5 Summary

In this chapter, we apply the MIMO coding techniques, STBC and VBLAST, to further enhance the goodput of the IEEE 802.11a system. Since the performances of STBC and VBLAST depend on different characteristics of the MIMO channel matrix. We have to adopt the RTS/CTS exchange to obtain the complete MIMO channel information and modify RTS, CTS, and data frame formats to carry the information for adaptive selection. The simulation results show that the MIMO system whose channel matrix has a larger minimum singular value utilizes the spectrum more efficiently. We

also compare the MIMO-enhanced 802.11a systems with standard IEEE 802.11a system using RTS/CTS access method. As expected, the MIMO coding techniques indeed upgrade the goodput of the IEEE 802.11a system.

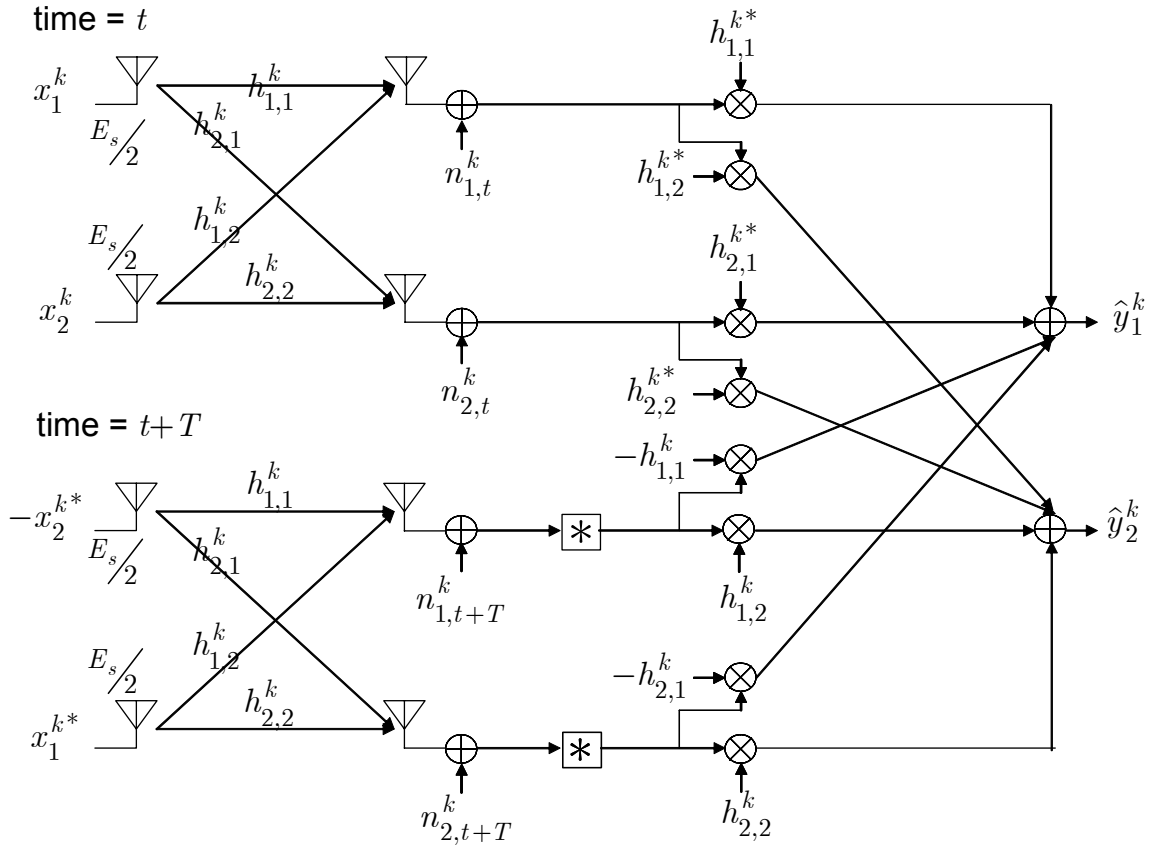

Figure 4.1: Linear combining for detection of STBC at *k*th subcarrier in 2x2 MIMO-OFDM systems

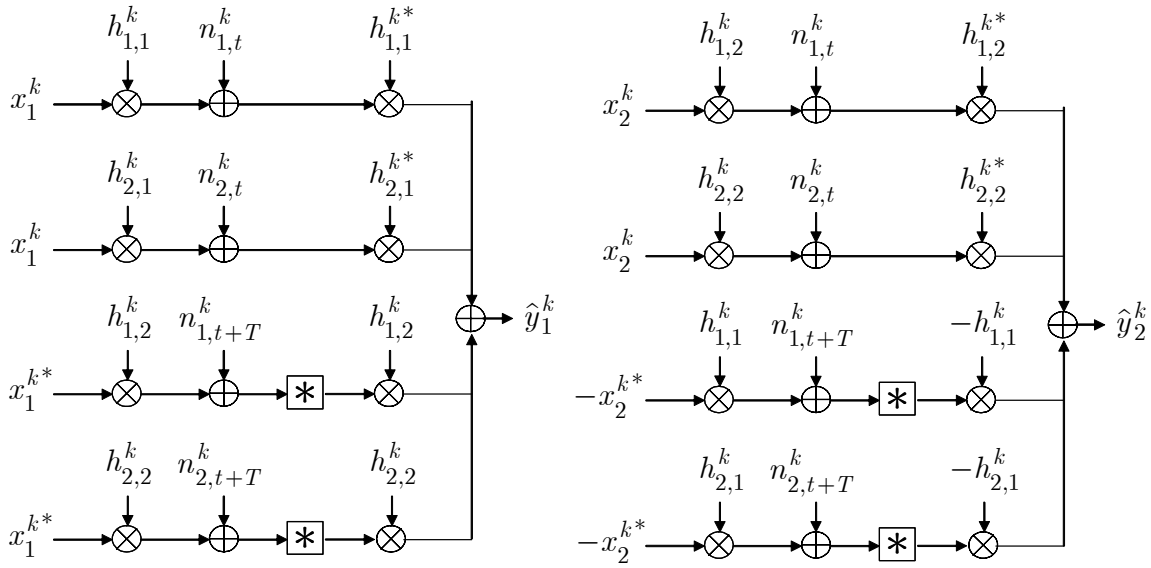

Figure 4.2: Equivalent maximum ration combining model for STBC at *k*th subcarrier in 2x2 MIMO-OFDM systems

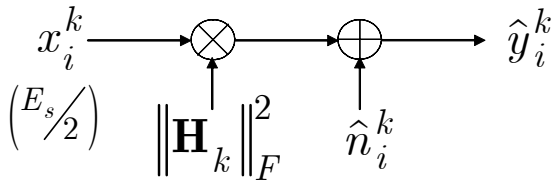

Figure 4.3: Equivalent scaled AWGN channel model for STBC at kth subcarrier in 2x2 MIMO-OFDM systems

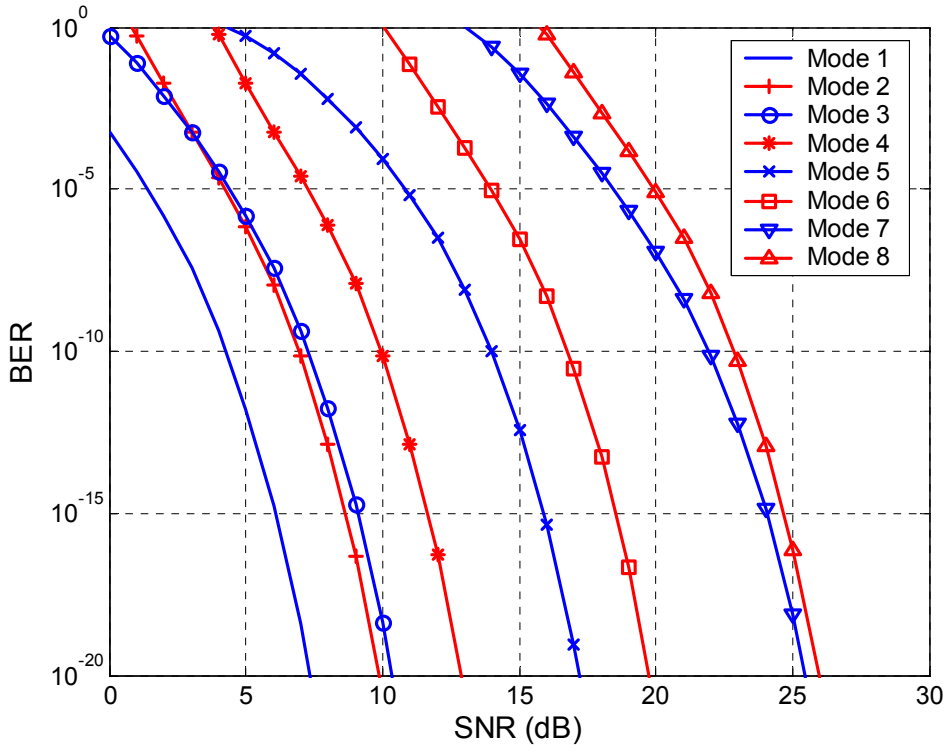

Figure 4.4: Instantaneous upper bound BER performance of eight PHY modes of STBC-enhanced 802.11a versus SNR (E_s/N_0)

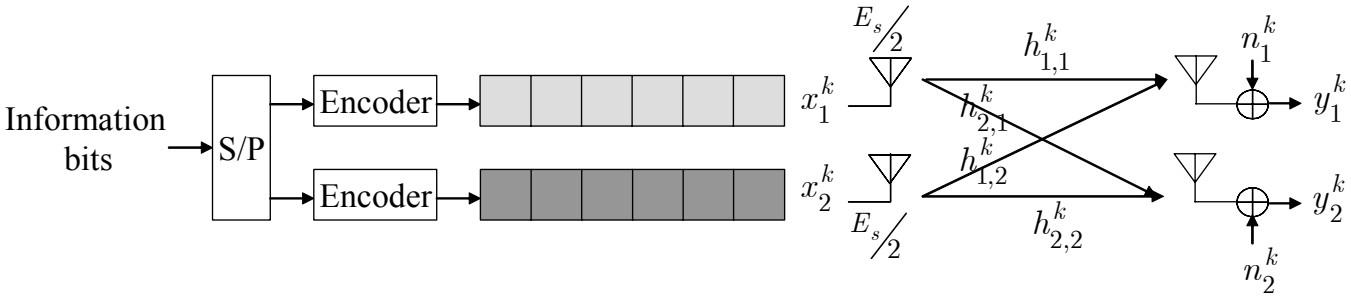

Figure 4.5: VBLAST architecture at *k*th subcarrier in 2x2 MIMO-OFDM systems

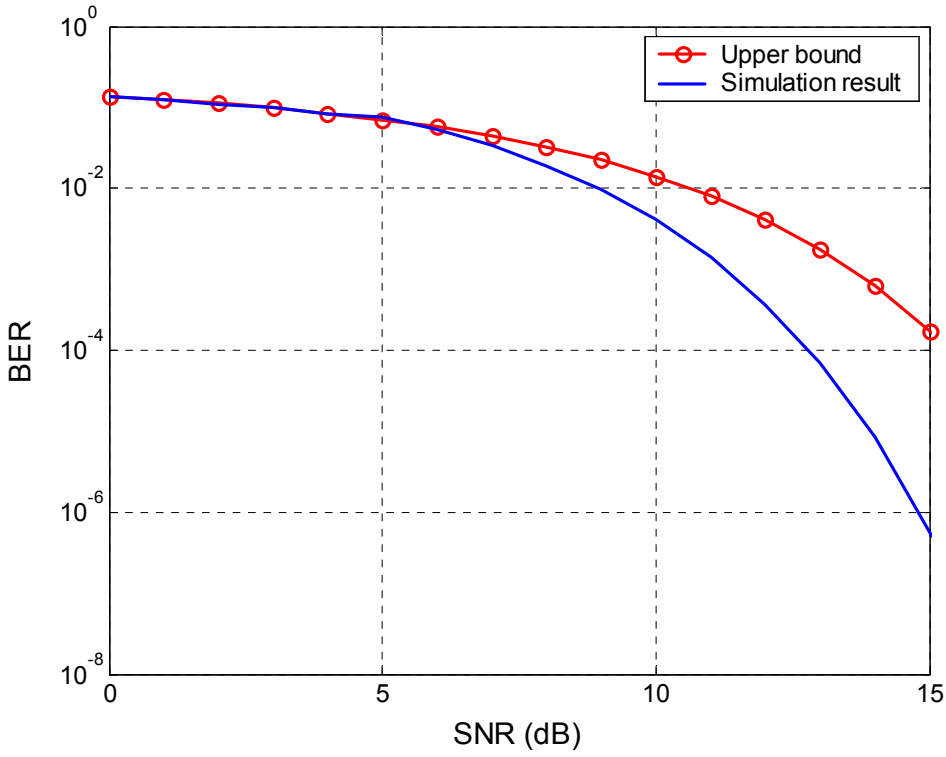

Figure 4.6: Instantaneous simulated and upper bound BER of VBLAST system with QPSK modulation versus SNR (E_s/N_0)

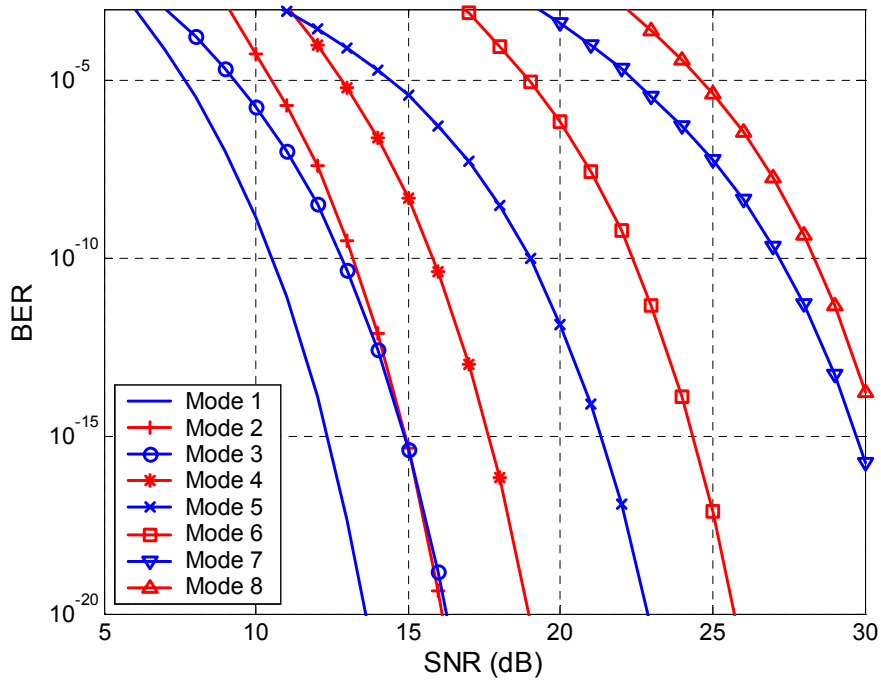

Figure 4.7: Instantaneous upper bound BER performance of eight PHY modes of VBLAST-enhanced 802.11a versus SNR (E_s/N_0)

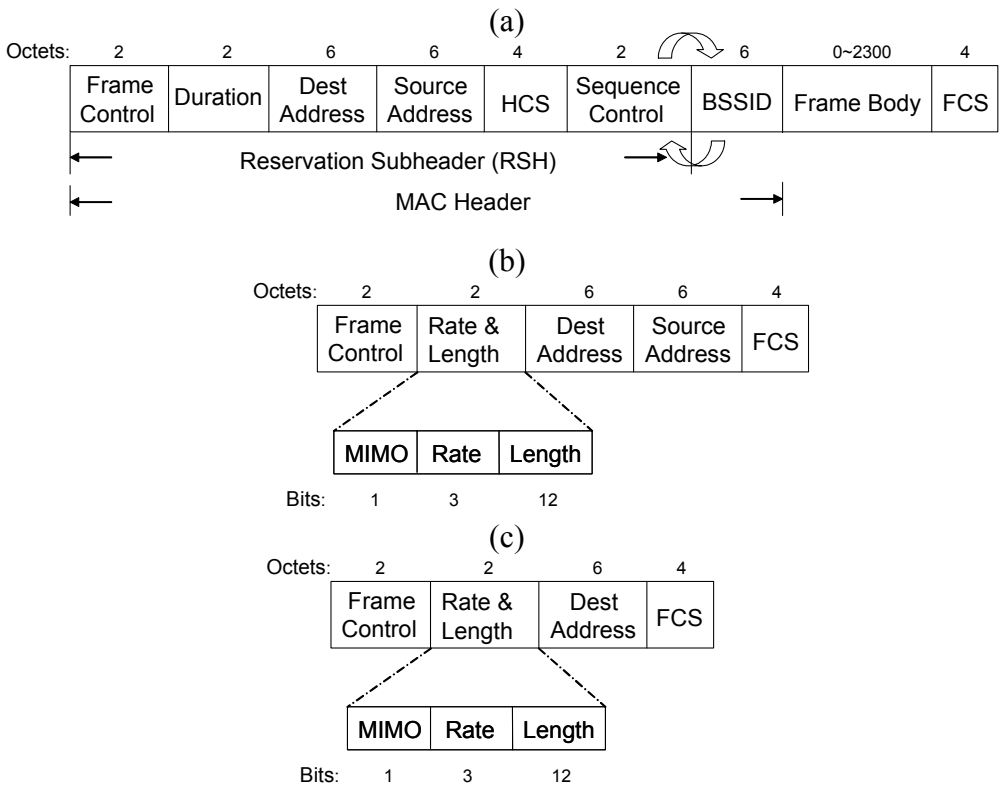

Figure 4.8: Modified frame formats of IEEE 802.11 MAC for link adaptation (a) Data frame (b) RTS frame (c) CTS frame

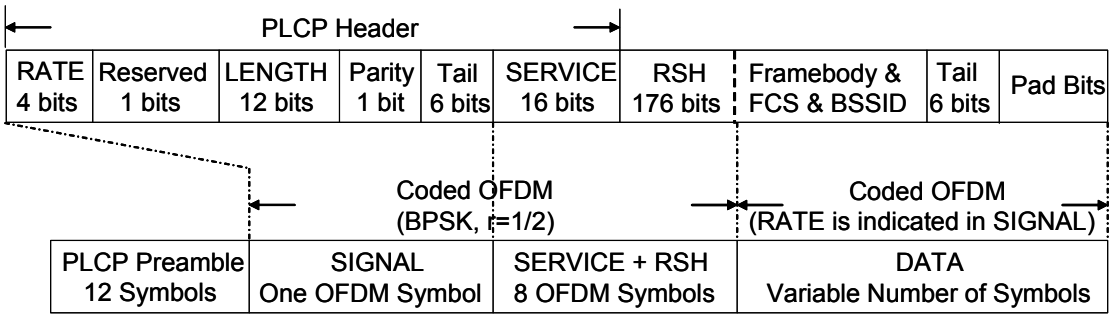

Figure 4.9: Modified PPDU frame format of IEEE 802.11a OFDM PHY for link adaptation

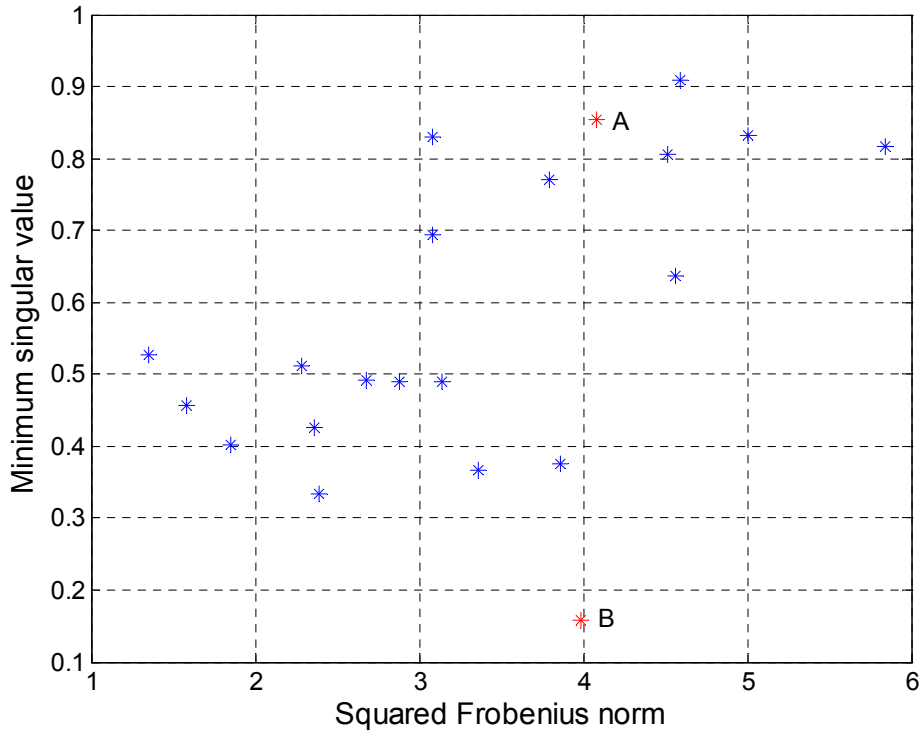

Figure 4.10: Distribution of squared Frobenius norm and minimum singular value generated by 20 independent flat Rayleigh fading 2x2 MIMO channel matrix

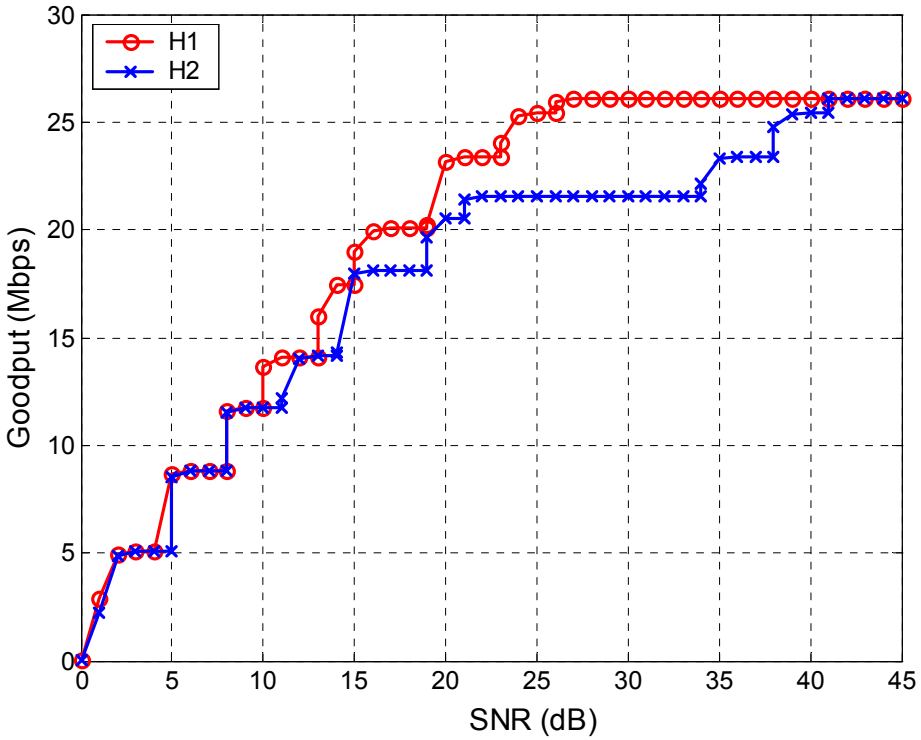

Figure 4.11: Maximum goodput for adaptive PHY mode and MIMO coding for 2x2 MIMO-enhanced 802.11a systems

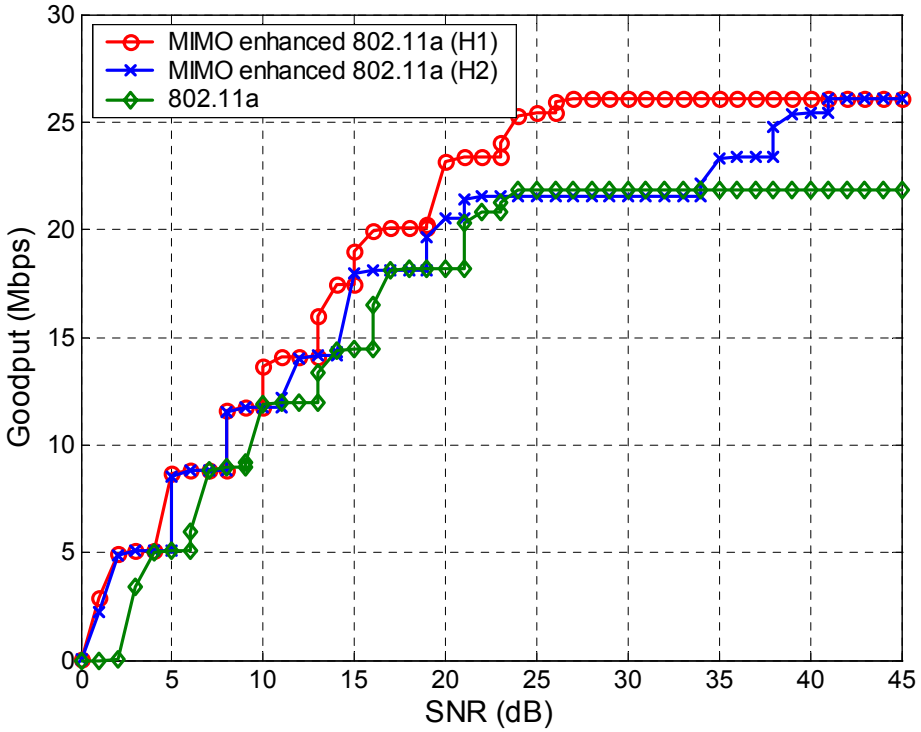

Figure 4.12: Maximum goodupt for adaptive PHY mode and MIMO coding for 2x2 MIMO-enhanced 802.11a systems and standard IEEE 802.11a system with $|h|^2 = 1$

Table 4.1: Contents of MIMO subfield in modified 802.11 MAC frame formats

MIMO Scheme	Contents
STBC	0
BLAST	1

Table 4.2: Contents of RATE subfield in modified 802.11 MAC frame formats

Rate (Mbps)	Contents
6	000
9	001
12	010
18	011
24	100
36	101
48	110
54	111

Table 4.3: Adaptive PHY mode and MIMO coding selection for 2x2 channel matrix with 2,000 MSDU and five contending stations. Deep color represents STBC while the light one stands for VBLAST

$\|\mathbf{H}\|_F^2 = 4.0822, \lambda_{\min} = 0.85341$

	Mode 1	Mode 3	Mode 4	Mode 3	Mode 4	Mode 5	Mode 6	Mode 7	Mode 8
SNR (dB)	~4	4~8	8~10	10~13	13~15	15~19	19~23	23~26	26~

Table 4.4: Adaptive PHY mode and MIMO coding selection for 2x2 channel matrix with 2,000 MSDU and five contending stations. Deep color represents STBC while the light one stands for VBLAST

$\|\mathbf{H}\|_F^2 = 3.9888, \lambda_{\min} = 0.15856$

	Mode 1	Mode 3	Mode 4	Mode 5	Mode 6	Mode 7	Mode 8	Mode 6	Mode 7	Mode 8
SNR (dB)	~5	5~8	8~11	11~14	14~19	19~21	21~34	34~38	38~41	41~

Chapter 5

Conclusion

In this thesis, the goodput performance is derived analytically for peer-to-peer communication with numbers of contending stations in the IEEE 802.11a DCF system. The effective goodput is expressed as a closed-form function of the data payload length, wireless channel condition, number of contending stations, and selected transmission rate for both the basic access method and RTS/CTS method. Assuming the availability of the wireless channel conditions and number of contending stations, we propose a link adaptation scheme which selects the best combination of the PHY mode and MAC mechanism based on the theoretical analysis. For instance, the higher rate PHY mode is chosen for good reception condition (high SNR value) because of its better goodput performance compared to the lower rate PHY mode and vice versa. But the selection of the MAC mechanisms requires more detailed information in addition to the channel condition. With regards to the data payload length, the longer it is the more demands of the RTS/CTS access method is required. The concept behind this fully agrees with the idea of using RTS_Threshold, the only parameter to decide as to whether the RTS/CTS access method is applied in former researches [2][3]. However, for the same data payload length, the use of the basic access method is preferable over the high-quality channel with higher rate PHY mode. Needless to say, the transmission duration of the data frame is the primary concern not the length. On the other hand, the

more contending stations in the network, the more potential collision events occur, thus the more likely the RTS/CTS access method is chosen.

Above-mentioned link adaptation scheme utilizes the MAC and PHY layers for achieving the optimum goodput in the inherent IEEE 802.11a WLANs. To further increase the link goodput, we introduce MIMO coding techniques, STBC and VBLAST, in Chapter 4. Through the performance analyses for both techniques, STBC gives an SNR gain (related to the squared Frobenius norm of the MIMO channel matrix) to enhance link reliability while VBLAST provides spectrum efficiency at the cost of poor error performance (related to the minimum singular value of the MIMO channel matrix). The RTS/CTS exchange is adopted to obtain complete channel information and perform link adaptation which selects the best combination of the MIMO coding technique and the PHY mode. The simulation results show that the MIMO system whose channel matrix has a larger minimum singular value utilizes the spectrum more efficiently since the VBLAST, which provides high spectrum efficiency, experiences fewer errors. We also compare the MIMO enhanced 802.11a systems with standard IEEE 802.11a system using the RTS/CTS access method. As expected, the MIMO coding techniques indeed upgrade the goodput of the 802.11a system.

The evaluated performance is based on the upper bound of error performance for VBLAST. Therefore, we underestimate the MIMO-enhanced 802.11a system to some degree. A more accurate performance analysis on VBLAST is a worthy research topic that can provide deeper insight and comprehensive understanding of the VBLAST-enhanced 802.11a. From another point of view on the MAC layer, the unavoidable overheads restrict the maximum goodput of the 802.11a WLANs. The ideas of frame aggregation and flow control can reduce the impact effectively. The frame aggregation scheme gathers several small data frames into one bigger data frame to reduce the amount of transmitted overheads. With the flow control scheme, nodes

with good channel conditions transmit the aggregated frames in burst while the nodes with bad channel condition buffer their data frames and perform frame aggregation.

However, the efforts for increasing the goodput for peer-to-peer communication may be in vain in the multihop scenarios unless routing protocols are able to take into account different channel conditions and transmission strategies. Because current routing protocols derive routes based on hop counts, the nodes farther apart with a poor channel condition communicate with each other at a lower data rate, thus poorer performance. Therefore, our future works shall include advanced subjects at PHY, MAC, and Network layers.

Bibliography

[1] IEEE 802.11, *Part 11: Wireless LAN medium access control (MAC) and physical layer (PHY) specifications*, Standard, IEEE, Aug. 1999.

[2] G. Bianchi, "Performance analysis of the IEEE 802.11 distributed coordination function," *IEEE Journal on Selected Area in Comm.*, vol. 18, no. 3, pp. 535-547, March 2000.

[3] P. Chatzmisios, V. Vitsas, and A. C. Bouncouvalas, "Throughput and delay analysis of IEEE 802.11 protocol," *Proc. 5th IEEE International Workshop on Networked Appliances*, Oct. 30-31, 2002.

[4] IEEE 802.11a, *Part 11: Wireless LAN, medium access control (MAC) and physical layer (PHY) specifications: high-speed physical layer in the 5GHz band*, supplement to IEEE 802.11 standard, Sept. 1999.

[5] B. Hirosaki, "An orthogonal multiplexed QAM system using the discrete Fourier transform," *IEEE Trans. on Comm.*, vol. 29, no. 7, pp. 982-989, July 1981.

[6] K. K. Leung and Li-Chun Wang, "Integrated link adaptation and power control for wireless IP networks," *Proc. IEEE VTC 2000*, vol. 3, pp. 2086-2092, Japan, May 2000.

[7] A. Kamerman and L. Monteban, "WaveLan II: A high-performance wireless LAN for the unlicensed band," *Bell Labs Technical Journal*, vol. 2, no. 3, pp. 118-133, Summer 1997

[8] G. Holland, N. H. Vaidya, and P. Bahl, "A rate-adaptive MAC protocol for multi-hop wireless networks," *Proc. ACM MobiCom '01*, pp. 236-251, July 2001.

[9] D. Qiao and S. Choi, "Goodput enhancement of IEEE 802.11a wireless LAN via link adaptation," *Proc. IEEE ICC '01*, vol. 7, pp. 1995-2000, June 2001.

[10] D. Qiao, S. Choi, and K. G. Shin, "Goodput analysis and link adaptation for IEEE 802.11a wireless LANs," *IEEE Trans. on Mobile Computing*, vol. 1, no. 4, pp. 278-292, Oct.-Dec. 2002.

[11] Jean-Lien C. Wu, Hunh-Huan Liu, and Yi-Jen Lung, "An adaptive multirate IEEE 802.11 wireless LAN," *Proc. International Conference on Information Networking '01*, pp. 411-418, Japan, Jan. 2001.

[12] G. J. Foschini and M. J. Gans, "On limits of wireless communications in a fading environment when using multiple antennas," *Wireless Personal Communications*, vol. 6, no. 3, pp. 311-335, March 1998.

[13] V. Tarokh, N. Seshadri, and A.R. Calderbank, "Space-time codes for high data rate wireless communication: performance criterion and code construction," *IEEE Trans. on Information Theory*, vol. 44, no. 3, pp. 744-756, March 1998.

[14] S. M. Alamouti, "A simple transmit diversity technique for wireless communications," *IEEE Journal on Selected Area in Comm.*, vol. 16, no. 8, pp. 1451-1458, Oct. 1998.

[15] V. Tarokh, H. Jafarkhani, and A. R. Calderbank, "Space-time block codes from orthogonal designs," *IEEE Trans. on Information Theory*, vol. 45, no. 5, pp. 1456-1467, July 1999.

[16] G. G. Rayleigh and J. M. Cioffi, "Spatio-temporal coding for wireless communication," *IEEE Trans. on Comm.*, vol. 46, no. 3, pp. 357-366, March 1998.

[17] A. van Zelst, "Space division multiplexing algorithms," *Proc. 10th Mediterranean Electrotechnical Conference*, vol. 3, pp. 1218-1221, Cyprus, May 2000.

[18] G. J. Foschini, "Layered space-time architecture for wireless communication in a fading environment when using multiple antennas," *Bell Lab. Tech. Journal*, vol. 1, no. 2, pp. 41-59, 1996.

[19] G. J. Foschini, G. D. Golden, R. A. Valenzuela, and P. W. Wolniansky, "Simplified processing for wireless communication at high spectral efficiency," *IEEE Journal on Selected Area in Comm.*, vol. 17, no. 11, pp. 1841-1852, Nov. 1999.

[20] R. van Nee, "A new OFDM standard for high rate wireless LAN in the 5 GHz band," *Proc. IEEE VTC '99*, vol. 1, pp. 258 –262, Sept. 1999.

[21] G. Bianchi, “IEEE 802.11 saturation throughput analysis,” *IEEE Comm. Letters*, vol. 2, no. 12, pp. 318-320, Dec. 1998.

[22] H. Wu, Y. Peng, K. Long, S. Cheng, and J. Ma, “Performance of reliable transport protocol over IEEE 802.11 wireless LAN: analysis and enhancement,” *Proc. IEEE INFOCOM ’02,* vol. 2, pp. 599-607, USA, June, 2002.

[23] J.G. Proakis, *Digital Communications*, 3rd edition, New York: McGraw-Hill, 1995.

[24] M. B. Pursley and D. J. Taipale, “Error probabilities for spread-spectrum packet radio with convolutional codes and viterbi decoding,” *IEEE Trans. on Comm.*, vol. 35, no. 1, pp. 1-12, Jan. 1987.

[25] D. Haccoun and G. Begin, “High-rate punctured convolutional codes for Viterbi and sequential decoding,” *IEEE Trans. on Comm.*, vol. 37, no. 11, pp. 1113-1125, Nov. 1989.

[26] P. Frenger, “Multi-rate convolutional codes,” *Tech. Report*, No. 21, Communication System Group, Chalmers University of Technology, Sweden.

[27] K. Fall and K. Varadhan, “NS notes and documentation,” LBNL, Aug. 1998. http://www-mash.cs.berkeley.edu/ns/.

[28] V. Tarokh, H. Jafarkhani, and A. R. Calderbank, “Space-time block coding for wireless communications: performance results,” *IEEE Journal on Selected Area in Comm.*, vol. 17, no. 3, pp. 451-460, March. 1999.

[29] S. Sandhu and A. Paulraj, “Space-time block codes: a capacity perspective,” *IEEE Comm. Letters*, vol. 4, no. 12, pp. 384-386, Dec. 2000.

[30] A. J. Paulraj, D. Gore, R. U. Nabar, and H. Bolcskei, “An overview of MIMO communications – a key to gigabit wireless,” *Proc. IEEE*, vol. 92, no. 2, pp.198-218, Feb. 2004.

[31] P. W. Wolniansky, G. J. Foschini, G. D. Golden, and R. A. Valenzuela, “V-BLAST: an architecture for realizing very high data rates over the rich-scattering wireless channel,” *Proc. ISSSE ’98*, pp. 295-300, Italy, Sept. 1998.

[32] G. D. Golden, G. J. Foschini, R. A. Valenzuela, and P. W. Wolniansky, “Detection algorithm and initial laboratory results using V-BLAST space-time communication architecture,” *IEE Letters*, vol. 35, no. 1, pp. 14-16, Jan. 1999.

[33] A. J. Paulraj, R. Nabar, and D. Gore, *Introduction to Space-Time Wireless Communications*, Cambridge: Cambridge University Press, May 2003.

[34] G. Burel, "Statistical analysis of the smallest singular value in MIMO transmission systems," *WSEAS ICOSSIP '02*, Greece, Sept. 2002.

[35] S. Nakao and Y. Doi, "Considerations for STS for MIMO-OFDM," SANYO Electric Co., Ltd. Japan, *Tech. Report*, IEEE 802.11-04/002r2, Jan. 2004.

[36] J. Boer, B. Driesen, and P. P. Giesberts, "Backwards compatibility: how to make a MIMO-OFDM system backwards compatible and coexistence with 11a/g at the link level," Agere Systems, *Tech. Report*, IEEE 802.11-03/714r0, Sept. 2003.